Atmos. Chem. Phys. Discuss., 15, 9107–9172, 2015
www.atmos-chem-phys-discuss.net/15/9107/2015/
doi:10.5194/acpd-15-9107-2015

Atmospheric Chemistry and Physics Discussions

The role of semi-volatile organic compounds in the mesoscale evolution of biomass burning aerosol: a modelling case study of the 2010 mega-fire event in Russia

I. B. Konovalov[1], M. Beekmann[2], E. V. Berezin[1,3], H. Petetin[2], T. Mielonen[4], I. N. Kuznetsova[5], and M. O. Andreae[6]

[1]Institute of Applied Physics, Russian Academy of Sciences, Nizhniy Novgorod, Russia
[2]Laboratoire Inter-Universitaire de Systèmes Atmosphériques, CNRS, Université Paris-Est and Université Paris 7, Créteil, France
[3]Lobachevsky State University of Nizhny Novgorod, Nizhny Novgorod, Russia
[4]Finnish Meteorological Institute, Kuopio, Finland
[5]Hydrometeorological Centre of Russia, Moscow, Russia
[6]Biogeochemistry Department, Max Planck Institute for Chemistry, Mainz, Germany

Received: 16 January 2015 – Accepted: 13 March 2015 – Published: 26 March 2015

Correspondence to: I. B. Konovalov (konov@appl.sci-nnov.ru)

Published by Copernicus Publications on behalf of the European Geosciences Union.

ACPD
15, 9107–9172, 2015

Abstract

Chemistry transport models (CTMs) are an indispensable tool for studying and predicting atmospheric and climate effects associated with carbonaceous aerosol from open biomass burning (BB); this type of aerosol is known to contribute significantly to both global radiative forcing and to episodes of air pollution in regions affected by wildfires. Improving model performance requires systematic comparison of simulation results with measurements of BB aerosol and elucidating possible reasons for discrepancies between them, which, "by default", are frequently attributed in the literature to uncertainties in emission data. Based on published laboratory data regarding atmospheric evolution of BB aerosol and by using the volatility basis set (VBS) approach to organic aerosol modeling along with a "conventional" approach, we examined the importance of taking gas-particle partitioning and oxidation of semi-volatile organic compounds (SVOCs) into account in simulations of the mesoscale evolution of smoke plumes from intense wildfires that occurred in western Russia in 2010. BB emissions of primary aerosol components were constrained with the PM_{10} and CO data from the air pollution monitoring network in the Moscow region. The results of the simulations performed with the CHIMERE CTM were evaluated by considering, in particular, the ratio of smoke-related enhancements in PM_{10} and CO concentrations (ΔPM_{10} and ΔCO) measured in Finland (in the city of Kuopio), nearly 1000 km downstream of the fire emission sources. It is found that while the conventional approach (disregarding oxidation of SVOCs and assuming organic aerosol material to be non-volatile) strongly underestimates values of $\Delta PM_{10}/\Delta CO$ observed in Kuopio (by almost a factor of two), the VBS approach is capable to bring the simulations to a reasonable agreement with the ground measurements both in Moscow and in Kuopio. Using the VBS instead of the conventional approach is also found to result in a major improvement of the agreement of simulations and satellite measurements of aerosol optical depth, as well as in considerable changes in predicted aerosol composition and top-down BB aerosol emission estimates derived from AOD measurements.

ACPD
15, 9107–9172, 2015

1 Introduction

Carbonaceous aerosol originating from open biomass burning (BB) plays a major role in the atmosphere by affecting both climate processes and air quality (Andreae and Merlet, 2001; Langmann et al., 2009). In particular, BB is estimated to provide about 40 % of the atmospheric budget of black carbon (BC) (Bond et al., 2013), which contributes significantly to climate forcing (IPCC, 2013; Andreae and Ramanathan, 2013). BB emissions are also known to be a major source of particulate organic matter (POM), which contributes to both direct and indirect radiative forcing by providing absorbing brown carbon (e.g., Chakrabarty et al., 2010; Saleh et al., 2014), enhancing light absorption by BC (up to a factor of two) due to the lensing effect (Jacobson, 2001), as well as contributing to the light scattering (Keil and Haywood, 2003). Episodes of a major impact of aerosol emissions from fires on the regional air quality have been reported worldwide (e.g., Heil and Goldammer, 2001; Sinha et al., 2003; Bertschi and Jaffe, 2005; Konovalov et al., 2011; Strand et al., 2012; Engling et al., 2014). Therefore, the physical and chemical properties of BB aerosol, and its sources and evolution have to be adequately represented in atmospheric numerical models aimed at analyzing and predicting climate changes and air pollution phenomena, (e.g., Kiehl et al., 2007; Goodrick et al., 2012).

Meanwhile, there are indications that the available chemistry transport models (CTMs) simulating sources and atmospheric evolution of BB aerosol are not always sufficiently accurate. For example, the concentrations of aerosol originating from wildfires in Central America were systematically underestimated (by about 70 %) in simulations performed by Wang et al. (2006) with the RAMS-AROMA regional transport model (in spite of the fact that the variability of the aerosol concentration was well captured in the simulations). Predictions of surface aerosol concentrations in California from the BlueSky Gateway (Strand et al., 2012) air quality modeling system were found to be in acceptable range of the observed values in one part of the model domain (specifically, in northern California), but negatively biased in the other part of the domain (in south-

ACPD
15, 9107–9172, 2015

ern California). Large regional biases in AOD simulations performed with the global GOCART CTM were found by Petrenko et al. (2012). Kaiser et al. (2012) found that in order to achieve a reasonable agreement of global simulations of aerosol optical depth (AOD) with corresponding satellite measurements, the BB aerosol emissions specified in the ECMWF integrated forecast system had to be increased globally by a factor of 3.4. Using AOD and carbon monoxide (CO) satellite measurements analyzed in combination with outputs of the mesoscale CHIMERE CTM, Konovalov et al. (2014) found (qualitatively similar to the results by Kaiser et al., 2012) that the ratios of aerosol and carbon monoxide emissions from forest and grassland fires in Siberia are likely to be about a factor of 2.2 and 2.8 larger than those calculated with typical emission factors from literature. In contrast, Konovalov et al. (2011) revealed that in order to fit the CHIMERE simulations to ground based observations during wildfires in western Russia, the BB aerosol emissions had to be scaled with a factor of about 0.5 relative to the CO emissions.

Although most modeling studies tend to attribute systematic discrepancies between simulations and atmospheric observations of BB aerosol to uncertainties in the fire emission inventories, it seems also quite probable that at least a part of the discrepancies may be due to deficiencies in the modeling representation of BB aerosol processes. Indeed, for the special case of organic aerosol (OA) originating from fossil fuel burning, it has been argued (e.g., Shrivastava et al., 2006; Donahue et al., 2006; Robinson et al., 2007) that adequate models of OA evolution require taking into account the volatility of primary OA (POA) compounds as well as formation of secondary OA (SOA) from oxidation of semi-volatile organic compounds (SVOC) in the atmosphere. Furthermore, laboratory measurements indicated that, like the POA emissions from fossil fuel burning, BB aerosol emissions feature a broad spectrum of volatility (e.g., Lipsky and Robinson, 2006; Grieshop et al., 2009b; Huffman et al., 2009; May et al., 2013) and may be subject to rapid oxidation processes leading to formation of substantial amounts of SOA (Grieshop et al., 2009a; Hennigan et al., 2011, 2012; Donahue et al., 2012; Ortega et al., 2013). An increase of BB aerosol mass or particle number concen-

ACPD
15, 9107–9172, 2015

tration was also diagnosed in some field studies (Hobbs et al., 2003; Yokelson et al., 2009; Akagi et al., 2012). Recently, Vakkari et al. (2014) showed evidence for substantial growth and increasing oxidation state of biomass burning aerosols during the first few hours of atmospheric transport. Meanwhile, all the chemistry transport models employed in the above mentioned simulations of BB aerosol evolution treated the primary aerosol emissions as non-volatile, and only oxidation of several definite volatile organic compounds (VOCs) was taken into account as a source of SOA in some of the models.

A general novel approach to OA modeling, known as the volatility basis set (VBS) approach, which is intended to represent the volatilities of a broad spectrum of primary organic compounds and their ageing processes in the atmosphere, was introduced by Donahue et al. (2006). Several studies applied this approach for modeling the evolution of OA from anthropogenic (fossil fuel burning) and (in some cases) biogenic emissions and found that it provides reasonable agreement between simulations and measurements (see, e.g., Lane et al., 2008; Murphy and Pandis, 2009; Farina et al., 2010; Hodzic et al., 2010; Tsimpidi et al., 2010; Shrivastava et al., 2011; Ahmadov et al., 2012; Zhang et al., 2013). Bergström et al. (2012) applied the VBS approach to modeling BB aerosol along with OA originating from predominantly anthropogenic and biogenic sources, but did not arrive at any unambiguous conclusion regarding an advantage of the VBS approach over a simpler ("conventional") one in the case of BB aerosol; note that their VBS scheme did not distinguish between the properties of OA from biomass burning and other sources.

The main goal of this study is to examine the impact of using the VBS approach instead of the conventional one on the simulated evolution of BB aerosol in an important (though episodic) situation when BB was a major source of OA. We parameterize the BB aerosol processes by using data of dedicated laboratory measurements and apply our model to the case of the mega-fire event that occurred in Western Russia in summer 2010 as a result of an abnormal heat wave (Barriopedro et al., 2011). This event provided abundant observational material for the critical evaluation of our current understanding of atmospheric effects of wildfires and has already received considerable

ACPD
15, 9107–9172, 2015

attention in the scientific literature (Elansky et al., 2011; Konovalov et al., 2011; Mei et al., 2011; Witte et al., 2011; Golitsyn et al., 2012; Huijnen et al., 2012; Krol et al., 2013; Popovicheva et al., 2014). However, to the best of our knowledge, there has been no study yet focusing on modeling the evolution ("ageing") of aerosol in BB plumes from these fires. By considering this special case, we intend to examine the feasibility and benefits of using the VBS approach for modeling aerosol evolution in BB plumes, especially at temporal scales considerably exceeding those addressed in typical laboratory measurements. In general, this study is intended to contribute to advancing current understanding of BB aerosol processes and their representation in chemistry transport models.

This paper is organized as follows: Sect. 2 describes our modeling framework; in particular, it outlines the methods and parameterizations representing BB aerosol emissions and evolution and defines the scenarios of our numerical experiments. Results of the numerical simulations are presented in comparison with data of in-situ and satellite measurements in Sect. 3, which also discusses the implications of the results of our simulations for predicting aerosol composition and estimation of emissions from wildfires by using the "top-down" approach. A summary of the results of this study and some concluding remarks are provided in Sect. 4.

2 Model and measurement data description

2.1 CHIMERE CTM: general characteristics

This study is based on using the CHIMERE CTM, which is a typical Eulerian off-line model designed for simulating and predicting air pollution at the regional and continental scales. It includes parameterizations of most important physical and chemical processes affecting the atmospheric evolution of aerosols of various types and origin (such as primary anthropogenic, dust, biogenic, sea salt, secondary inorganic and organic aerosols) and gaseous air pollutants. These processes include, in par-

ACPD
15, 9107–9172, 2015

ticular, emissions of gases and aerosols (the anthropogenic and biogenic emission interfaces enable calculation of the corresponding emissions on a model grid from data of corresponding emission inventories), chemical transformation of tens of compounds due to gas-phase and heterogeneous reactions, absorption/desorption of some semi-volatile species by/from aerosol particles, advection and turbulent mixing of gases and aerosols, and their dry and wet deposition. The detailed description of CHIMERE and examples of its numerous applications are provided in Menut et al. (2013) and in the CHIMERE documentation available online along with the model codes at http://www.lmd.polytechnique.fr/chimere.

While most earlier CHIMERE applications addressed contributions to atmospheric composition from anthropogenic and biogenic sources, it was also successfully applied in several studies focusing on the atmospheric effects of fire emissions (Hodzic et al., 2007; Konovalov et al., 2011, 2012, 2014; Péré et al., 2014). In particular, simulations performed with CHIMERE were found by Konovalov et al. (2011) to be in good agreement with air quality monitoring data in Moscow during the extreme air pollution event caused by wildfires in 2010. The same event and similar data are considered in this study. The CHIMERE configuration is similar to that in the studies by Konovalov et al. (2011, 2014), except for some changes and updates mainly applied to our method aimed at deriving fire emissions from satellite measurements of fire radiative power (FRP) (Ichoku and Kaufman, 2005).

2.2 Basic model configuration

Gas-phase processes were simulated with the reduced chemical mechanism MELCHIOR2 (Derognat et al., 2003; Menut et al., 2013) including about 120 reactions of 40 species. Menut et al. (2013) found that the performance of this computationally efficient mechanism in the case of ozone simulations was very similar to that of a much more complex mechanism, such as SAPRC07 (Carter, 2010). Photolysis rates were calculated with the TUV model (Madronich et al., 1998) embedded in CHIMERE as a function of AOD derived from Moderate-resolution Imaging Spectroradiometer

ACPD
15, 9107–9172, 2015

(MODIS) measurements (see Konovalov et al., 2011, for further detail). Evolution of secondary inorganic aerosol was simulated with the tabulated version of the thermodynamic model ISORROPIA (Nenes et al., 1998). Anthropogenic emissions of gases and aerosol were specified by using the EMEP (European Monitoring and Evaluation Programme) inventory data (EMEP/CEIP, 2014) for the year 2010. Anthropogenic primary aerosol emissions were distributed among nine size bins with diameters from 20 nm to 10 µm by assuming a bimodal log-normal distribution with a mean and SD of 0.11 µm and 1.6 for the fine mode and of 4 µm and 1.1 for the course mode, respectively (accordingly to the CHIMERE standard settings). Biogenic emissions (including those of aerosol precursors) were calculated by using the standard CHIMERE interface and data by the MEGAN (Model of Emissions of Gases and Aerosols from Nature) model (Guenther et al., 2006) for emissions from vegetation, and the European inventory of soil NO emissions by Stohl et al. (1996). Dust aerosol emissions were taken into account by using a simple parameterization developed by Vautard et al. (2005). The monthly climatological data from the LMDz-INCA global model (Folberth et al., 2006) were used as initial and boundary conditions for our simulations.

Apart from using the standard model output data for concentrations of gaseous and aerosol species, we considered AOD at 550 nm; it was evaluated in the same way as in Konovalov et al. (2014) following a robust method, proposed by Ichoku and Kaufman (2005). Specifically, AOD was derived from simulated aerosol mass column concentrations by applying the mass extinction efficiency coefficient. We took into account that a predominant part of atmospheric aerosol loading in the situation considered was due to biomass burning and chose this coefficient, using the experimental data by Reid et al. (2005), to be the same as in Konovalov et al. (2014) ($4.7 \pm 0.8\,m^2\,g^{-1}$). Some bias in AOD values calculated in this way may be associated with small (in the case considered) contributions of anthropogenic, biogenic, and dust aerosols, whose mass extinction efficiency is different from that of BB aerosol. We evaluated this bias as the mean relative difference between the simulated and measured AOD in the grid cells on the days where and when the contribution of BB aerosol was negligible (see Konovalov

ACPD
15, 9107–9172, 2015

et al., 2014, for further detail); the bias was then subtracted from the simulated AOD values.

The WRF-ARW (v.3.6) model (Skamarock et al., 2005) was used as a meteorological driver for CHIMERE. The meteorological data were calculated on a 50 km × 50 km grid with 30 levels extending in the vertical up to the 50 hPa pressure level. The Mellow–Yamada–Janjic (Eta) scheme (Janjic, 1994) was used for the simulation of boundary layer processes together with the Eta similarity scheme (based on the Monin–Obukhov theory) for surface physics (Janjic, 1990).

The evolution of BB plumes was simulated with a resolution of 0.5 by 0.5 ° and twelve layers in the vertical; the upper layer corresponded to the 200 hPa pressure level. The study region (corresponding to the model domain) covers most of European Russia and a part of Eastern Europe (48–66° N; 20–56° E). The simulations were performed for the period from 12 July to 20 August 2010. The first three days were reserved for the model's "spin-up"; therefore, the period of our analysis began on 15 July.

2.3 Fire emissions

Below, we outline our calculations of fire emissions by paying special attention to changes with respect to the previous studies, where a similar method was used. Fire emissions for a species s at time t, $E^s(t)$ (g s^{-1} m^{-2}), were calculated as follows:

$$E^s(t) = \Phi_d \sum_l \alpha \beta_l^s \rho_l h_{el}(t) C(\tau), \quad (1)$$

where Φ_d (W m^{-2}) is the daily mean FRP density derived from daily maximums of FRP in a given cell of the model grid, α (g[dry biomass] s^{-1} W^{-1}) is the factor converting FRP to the biomass burning rate (BBR) (below, we refer to this factor as the FRP-to-BBR conversion factor) for a given land cover type l, β_l^s (g[model species] g^{-1}[dry biomass]) are the emission factors, ρ_l is the fraction of the land cover type l, h_{el} is the assumed diurnal variation of fire emissions, and C is an additional ad hoc correction factor specified as a function of AOD at 550 nm wavelength, τ. This relationship follows a popular

ACPD
15, 9107–9172, 2015

approach to calculation of fire emissions, which was proposed by Ichoku and Kaufman (2005) and has been used in a number of studies (see, e.g., Sofiev et al., 2009; Kaiser et al., 2012; Konovalov et al., 2014, and references therein) since then. The factor C, which was initially introduced in Konovalov et al. (2011), is intended to compensate for a possible attenuation of FRP measured from satellites by very heavy smoke from intense fires in the region and period considered; it is also assumed to account for the part of emissions from peat fires invisible from space but coinciding with visible forest or grass fires.

For convenience, we express the factor α (below, we refer to this factor as the FRP-to-BBR conversion factor) as the product of its "a priori" value, α_0, and the "a posteriori" correction factor, F_α:

$$\alpha = \alpha_0 F_\alpha. \tag{2}$$

Taking into account the experimental data by Wooster et al. (2005), α_0 is taken to be 3.68×10^{-4} g[dry biomass] s^{-1} W^{-1}, and different estimates of F_α are inferred from atmospheric measurements as explained in Sect. 2.6.

Similar to Konovalov et al. (2011, 2014), the daily mean FRP density is evaluated by selecting daily maxima of the FRP density in each model grid cell and by scaling them with the assumed diurnal cycle of the FRP maxima, h_{ml}:

$$\Phi_{\mathrm{d}} = \frac{\max\{\Phi_k, k = 1, \ldots K\}}{\sum \rho_l h_{\mathrm{ml}}(t_{\max})} \tag{3}$$

where k is the satellite orbit index, h_{ml} is the assumed diurnal distribution of the FRP daily maximums, and $t_{\max}$ is the moment of time when the daily maximum of FRP is observed. The initial calculations of fire emissions were made on a grid of a higher resolution (0.25 by 0.1 °) to minimize the effect of cloud and smoke contamination on the selected FRP daily maximum values; these emission data were then projected onto the model grid. The temporal resolution of the emission data was 1 h.

ACPD
15, 9107–9172, 2015

While Eq. (1) in combination with Eq. (2), is very similar to Eq. (5) in Konovalov et al. (2011), there are a few noteworthy differences between them. First, in this study, we do not consider the peat fires explicitly. Although the attempt to estimate the emissions from peat fires (not visible from space), as described in Konovalov et al. (2011), was rather successful, this estimation was associated with a large uncertainty, which would only hinder evaluation of different modeling scenarios in this study. Note, however, that we still take peat fires into account implicitly by adjusting the FRP-to-BBR conversion factor. For similar reasons, we assume that the same FRP-to-BBR conversion factor value (and the same value of the correction factor, F_α) is applicable to both forest and grass fires (visible from space).

Second, for convenience, we normalize the factor $C(\tau)$ such that its average over the whole study region is equal to unity. Note that, following Konovalov et al. (2011), we define $C(\tau)$ to be proportional to $\exp(\tau)$; introducing this factor was found to drastically improve the agreement of our simulations with air pollution measurements in Moscow.

Third, instead of assuming very strong diurnal variation of fire emissions (see Konovalov et al., 2011, and Fig. 1 therein), we derived the diurnal cycle of the emissions directly from FRP observations using the method and formulations proposed by Konovalov et al. (2014) (see Eqs. 5 and 6 therein). In this study, we attempted to advance this method further by distinguishing between the diurnal cycle of FRP daily maximums, h_{ml}, and that of emissions, h_{el}. To estimate the latter, the formulations given in Konovalov et al. (2014) were applied to all available FRP data, while the former was derived only from FRP daily maximums (exactly in the same way as in Konovalov et al. (2014), where h_{el} was implicitly assumed to be equal to h_{ml}). The diurnal cycles specified in this study for agricultural and grass fires, and (separately) for forest fires are shown in Fig. 1. Finally, the emission factors for organic carbon (OC), BC, CO, NO_x, and non-methane hydrocarbons (NMHC) (see Table 1) were specified using an updated dataset (M.O. Andreae, unpublished data, 2014; Andreae and Merlet, 2001); emissions of individual VOCs were calculated by distributing the total NMHC emissions among the compounds represented in this database (proportionally to the measured

ACPD
15, 9107–9172, 2015

emission factors of these compounds) and then aggregating them into eleven lumped model species (similarly as it is done in the CHIMERE emission interface for anthropogenic emissions, see Menut et al., 2013). POM emissions are obtained by scaling the OC emissions with a factor of 1.8, taking into account the range of OC/POM ratios observed in fire plumes and assumed in fire emission inventories (e.g., Alves et al., 2011; van der Werf et al., 2010).

Similar to Konovalov et al. (2014), the injection of fire emissions into the atmosphere was simulated by using the parameterization proposed by Sofiev et al. (2012). This parameterization enables evaluation of maximum plume height as a function of the FRP measured in a given fire pixel and of the Brunt–Väisälä frequency in the free troposphere. We consider this method as advantageous over a simpler method (assuming uniform distribution of fire emissions up to the height of one kilometer), which was employed in Konovalov et al. (2011), although no significant differences between results obtained with these two methods were revealed in the case of Siberian fires (Konovalov et al., 2014). We would like to emphasize that the changes in our calculations of fire emissions with respect to the previous studies affected the model performance only slightly and could not influence the major conclusions of this study.

2.4 Representation of BB OA processes in CHIMERE

In this study, we employ two different methods for modelling BB OA evolution. The first method is used in the standard version of CHIMERE. The second method is based on the VBS approach (Donahue et al., 2006; Robinson et al., 2007; Lane et al., 2008) and was initially implemented in dedicated versions of CHIMERE for the case of OA originating from fossil fuel burning and biogenic emissions (Hodzic et al., 2010; Zhang et al., 2013). A description of these methods given below focuses on their application to modelling of BB aerosol.

ACPD
15, 9107–9172, 2015

2.4.1 "Standard" method for organic aerosol

Aerosol particles emitted from fires are conventionally assumed to consist of non-volatile POM and BC. Therefore, they cannot evaporate and can be lost only as a result of deposition and transport outside of the model domain. Primary OA emissions are distributed according to a lognormal size distribution with a mean diameter of 2 µm and a SD of 1.6 by taking into account fresh smoke observations reported in the literature (see, e.g., Fiebig et al., 2003). A coarse fraction of primary aerosol particles having a typical mean diameter of about 5 µm and usually contributing 10–30 % to the total mass of fresh aerosol emissions (and, probably, even a smaller part of organic carbon as indicated, e.g., by Alves et al., 2011) was disregarded to facilitate the comparative analysis of simulations performed with the standard and VBS method.

The formation of SOA is represented by absorption of SVOCs produced as a result of oxidation of primary VOCs (Bessagnet et al., 2009; Hodzic et al., 2009). The yield of SVOCs from oxidation of VOCs from both fossil fuel and biomass burning is described by a single-step oxidation mechanism (Pun et al., 2006) as reactions of three lumped model VOC species (SVOC precursors) with OH, O_3 and NO_3 producing several surrogate SVOC species. These three lumped species are assumed to represent three classes of VOCs, such as a class of alkanes from C4 to C13, a class of mono-substituted aromatics including benzene, and a class of polysubstituted aromatics. The same single-step oxidation mechanism by Pun et al. (2006), with some modifications introduced following the formulations by Kroll et al. (2006) and Zhang et al. (2007), is used to represent the formation of SVOC as a result of oxidation of biogenic VOCs (for isoprene and terpenes). Further details regarding the representation of OA processes in the standard version of CHIMERE can be found elsewhere (Bessagnet et al., 2009; Hodzic et al., 2009; Menut et al., 2013).

ACPD
15, 9107–9172, 2015

2.4.2 Volatility Basis Set (VBS) method

Here, POA emissions (including all organic material that is assumed to have a potential to form OA particles under atmospheric conditions) are considered as semi-volatile and distributed into several volatility classes characterized by the reference saturation concentration C_i^* at 298 K, enthalpy of vaporization, ΔH_i, and the fraction in the total POA emissions, f_i (where i is the index of a volatility class). The emission factors for total POA emissions, β^{poa}, and for organic carbon in particles (OC), β^{oc}, are assumed to be related as predicted by partitioning theory (Pankow, 1994; Shrivastava et al., 2006):

$$\beta^{poa} = \beta^{oc}\eta\left[\sum_i f_i\left(1+\frac{C_i^*\exp\left(-\frac{\Delta H_i}{R}\left(\frac{1}{T}-\frac{1}{298}\right)\right)\frac{298}{T}}{C_{OA}}\right)^{-1}\right]^{-1}, \quad (4)$$

where C_{OA} and T are the ambient OA mass concentration and temperature, R is the gas constant, and the factor η (assumed to be equal 1.8 here) is applied to convert OC into POM. In Eq. (4), the larger the ambient concentration C_{OA} and the smaller the saturation concentration C_i^*, the larger is the fraction of POA emissions in the particle phase, and thus the closer the ratio β^{poa} over $\beta^{oc}\eta$ is to unity. In contrast, for small C_{OA} and large C_i^*, a large part of POA emissions occurs in the gas phase and is not accounted for in measurements of particulate phase emissions. While the factors β^{oc}, characterizing emissions of OC from biomass burning, have been frequently measured both in laboratory and field studies (see, e.g., Akagi et al., 2011, and references therein) and are widely used in emission inventories (see, e.g., van der Werf et al., 2010), their values reported in the literature are usually not accompanied by corresponding data regarding C_{OA} and ambient temperature. Note that disregarding the gas-particle conversion processes may account for a part of the large discrepancies between different measurements of the emission factors. Therefore, some additional assumptions were

ACPD
15, 9107–9172, 2015

needed. Specifically, we assumed that $T = 298\,\mathrm{K}$ and $C_{OA} = 10\,\mathrm{mg\,m^{-3}}$. For comparison, Vicente et al. (2013) reported that $PM_{2.5}$ concentrations during their emission factor measurements in the vicinity of wildfires in Portugal were in the broad range from 0.69 to $25\,\mathrm{mg\,m^{-3}}$. In addition, we assumed that all POA were released into the atmosphere from fires as particles (as a result of the condensation process under very high ambient concentration of combustion products after their initial cooling). These assumptions do not have a significant effect on our simulations because the total BB aerosol emissions were constrained by measurements, as explained in Sect. 2.6.

Volatility distributions of POA were specified by using the results of a dedicated laboratory study by May et al. (2013), in which a kinetic model was used to derive volatility distributions and enthalpies of vaporization from thermodenuder measurements of BB emissions. Unfortunately, the derived volatility distributions are characterized by very large uncertainties (which likely reflect a part of the natural variability of volatility of smoke from burning of different types of biomass) and depend, in particular, on the assumed value of the mass accommodation coefficient. We tried to take into account this uncertainty by considering two simulation scenarios with different volatility distributions described in Sect. 2.7. POA emissions were distributed among nine size sections according to the same size distribution as described above for the standard method (see Sect. 2.4.1).

To improve the consistency of our model with the kinetic model used by May et al. (2013) for volatility estimations, we slightly modified the kinetic part of the absorption scheme in CHIMERE. Specifically, we replaced the formulation of the absorption process based on Bowman et al. (1997) with an approximation based on the Fuchs–Sutugin interpolation formula Seinfeld and Pandis (2006). In addition, to insure numerical stability of our calculations, evaporation of POA in the two lowest volatility classes (with $C^* = 0.01\,\mu\mathrm{g\,m^{-3}}$ and $C^* = 0.1\,\mu\mathrm{g\,m^{-3}}$) was disabled. This restriction did not affect our results, since typical OA concentrations in the smoke plumes considered were much higher ($> 10\,\mu\mathrm{g\,m^{-3}}$) even after strong dilution.

ACPD
15, 9107–9172, 2015

The POA were assumed to be subject to gas-phase oxidation, which was represented by the reaction of POA with OH. The oxidation mechanism was parameterized in two different ways. First, based on the estimates derived by Grieshop et al. (2009a) from laboratory measurements of the oxidation of BB smoke from a wood stove, each reaction was assumed to reduce the volatility of organic gases (from a given volatility class) by a factor of 100 (leading to a two-bin shift in the volatility distribution) and to increase the organic compound mass by 40 %; the reaction rate constant was set to be 2×10^{-11} cm^{-3} molecules^{-1} s^{-1} except for a test scenario (see Sect. 2.7) in which the rate was doubled. Evolution of oxygenated POA (OPOA) produced in the reaction of POA with OH was simulated in the same way as that of POA (that is, OPOA were governed by partitioning theory and experienced successive oxidation at the same rate and mass increment as POA). Second, the SOA formation from SVOCs was parameterized using a "surrogate species" representing a mixture of numerous organic compounds unspecified in available emission inventories, as proposed recently by Jathar et al. (2014). The parameterization, which had been obtained by fitting box model simulations to the data of the biomass burning laboratory experiments described in Hennigan et al. (2011), represents the POA oxidation as a single-generation process (associated with a minor net loss of the total mass of POA and OPOA species) and assumes that the VBS SOA yields from the POA oxidation are similar to those from oxidation of n-pentadecane (C_{15} n-alcane). Accordingly, we assumed the same OPOA mass yields as those given in Jathar et al. (2014) (see Table S3 therein). In addition, consistently with the analysis in Jathar et al. (2014), we assumed that n-pentadecane represents not only POA species, but also a fraction (10 %) of the total NMHC emissions from biomass burning. Note that the experimental data by Hennigan et al. (2011) are likely more representative of a range of real biomass burning conditions (at least, in North America) than those obtained and analyzed by Grieshop et al. (2009a). Nonetheless, it was difficult to predict a priori which of the parameterizations would enable the best performance of our simulations in the special case analyzed in this study. Indeed, on the one hand, the range of conditions reproduced in our simulations significantly

ACPD
15, 9107–9172, 2015

surpassed that addressed in the laboratory experiments. In particular, aerosol concentrations were typically much higher (up to almost 3000 $\mu g\,m^{-3}$) and duration of the aerosol evolution was much longer in the simulations (more than one day), compared to those in the laboratory experiments (about 100 $\mu g\,m^{-3}$ and less, and several hours, respectively). Besides, ageing of aerosol emissions from many kinds of "fuels" typical for European Russia (e.g. Scotch pine, Norway spruce, elm, birch, etc.) has not yet been investigated in laboratories. On the other hand, even the laboratory studies (Jathar et al., 2014; Grieshop et al., 2009a) indicated a large variability of the SOA yields in separate experiments, which was not reproduced by box models employing the parameterizations outlined above.

Note that the substantial increase of BB aerosol mass due to oxidation processes was also found in laboratory experiments by Ortega et al. (2013); however, their data were not fitted to VBS models (unlike the measurements in Hennigan et al., 2011 and Grieshop et al., 2009a) and thus were less suitable for configuring our simulations. Note also that using a more complex representation of BB OA evolution, e.g., involving a two-dimensional VBS scheme (Donahue et al., 2012) and taking into account such a potentially important process as fragmentation (Chacon-Madrid and Donahue, 2011), was not feasible in this study due to the lack of robust experimental data and the absence of suitable parameterizations.

Along with SOA formation resulting from the absorption of OPOA, we took into account a minor (under conditions of this study) SOA source associated with oxidation of "traditional" SOA precursors. A modelling scheme accounting for this source was adapted from Zhang et al. (2013): it simulates the formation of SOA from oxidation of anthropogenic VOCs by using six lumped species representing SOA precursors and four volatility classes. The BB emissions of these lumped SOA precursors were aggregated from emissions of individual VOCs using the data of Andreae and Merlet (2001) with recent updates (in the same way as the emissions of other model organic species).

ACPD
15, 9107–9172, 2015

2.5 Measurement data

Similar to Konovalov et al. (2011), we used the CO and PM_{10} measurements at the automatic air pollution monitoring stations of the State Environmental Institution "Mosecomonitoring" for calibration of fire emissions. We selected only those sites that provided both CO and PM_{10} data for at least 50 % of days during the period addressed in this study (from 15 July to 20 August 2010). These criteria were satisfied for four sites, including those located inside of the city of Moscow ("Kozhuhovo", "MGU") and in Moscow's suburbs ("Pavlovskii posad" and "Zelenograd"). The selected stations were equipped with Thermo TEOM1400a and OPTEK K-100 commercial devices based on the Tapered Element Oscillating Microbalance and electrochemical methods employed for PM_{10} and CO measurements, respectively. The measurements were nominally taken three times per hour.

Along with the air pollution data from the Moscow region, we used simultaneous CO and PM_{10} measurements from the city of Kuopio, Finland (Portin et al., 2012). A Thermo TEOM 1400a and Monitor Labs 9830 B IR absorption CO analyzer were used for PM_{10} and CO measurements, respectively. By comparing relative perturbations of PM_{10} and CO in the Moscow region (that is, near the fires) and in Kuopio (situated about 1000 km from Moscow), we attempt to elucidate the changes in BB aerosol mass due to transformation and loss processes in the atmosphere. The CO and PM_{10} measurements in Kuopio were earlier found to reflect large air pollution events associated with transport of smoke plumes from fires in Russia to Finland (Portin et al., 2012; Mielonen et al., 2011). The contribution of BB emissions was clearly distinguishable against "background" conditions in Kuopio, particularly because the air pollution level there is typically very low. Although the city of Kuopio has several sites for PM_{10} measurements, only one site (Maaherrankatu) provided data from both CO and PM_{10} measurements; therefore, the data from only this site were used for quantitative evaluation of our model performance.

ACPD
15, 9107–9172, 2015

The observational data were averaged on a daily basis (the days were defined in UTC) and matched to the daily mean simulated concentrations from grid cells covering the locations of the stations. The observational (or simulated) data for the selected sites in the Moscow region for a given day were combined by averaging.

We also evaluated our simulations against aerosol optical depth (AOD) retrieved from MODIS measurements onboard the AQUA and TERRA satellites; the AOD data (Remer et al., 2005; Levy et al., 2010) with the spatial resolution of $1^\circ \times 1^\circ$ were obtained as the L3 MYD08_D3/MOD08_D3 data product from the NASA Giovanni-Interactive Visualization and Analysis system (http://daac.gsfc.nasa.gov/giovanni/). The MODIS AOD daily data were matched to the simulated AOD values re-gridded to the $1^\circ \times 1^\circ$ grid and averaged over the period from 10 to 14 h of local solar time (that is, over the period of daytime satellite overpasses). The same measurement data were introduced after additional spatial and temporal interpolation (Konovalov et al., 2011) into the TUV model, which (as noted above) was used to calculate the photolysis rates in CHIMERE.

2.6 Optimization of fire emissions

We calibrated the fire emissions by estimating the correction factor, F_α, involved in the relationship between FRP and the emissions (see Eqs. 1 and 2). Different estimates of F_α were derived independently from CO and PM_{10} measurements by minimizing the following cost function, J:

$$J = \sum_{i=1}^{N_d} \theta^i \left(V_m^i - V_o^i - \Delta \right)^2, \quad (5)$$

where V_m and V_o are the modelled and observed daily concentrations of CO or PM_{10}, i is the index of a day, N_d is the total number of days in the period considered, θ_i is the operator equal to unity for days affected by fires (here, those were the days when the relative contribution of fire emissions to the simulated CO concentration exceeded 10 %) and zero otherwise, and Δ is the bias which was estimated as the mean dif-

ACPD
15, 9107–9172, 2015

ference between measurements and simulations on days featuring "background" air pollution conditions (i.e., when θ_i was set to be zero).

The initial estimate of F_α was derived, under the assumption of linear dependence of V_m on F_α, from results of "twin" simulations performed with $F_\alpha = 0$ and $F_\alpha = 1$. To achieve higher accuracy in the case when the estimation of F_α involved aerosol data from VBS simulations, the estimation procedure was re-iterated using a model run with F_α derived from the initial twin experiment. Otherwise (for the cases when the estimate of F_α was obtained either from CO data or using the "standard" aerosol scheme), the additional iteration was not necessary because the nonlinearity of a relationship between fire emissions and aerosol concentrations was negligible (similarly to the cases discussed in Konovalov et al., 2011 and Konovalov et al., 2014). The uncertainty in F_α was estimated from results of the Monte-Carlo experiment involving bootstrapping of the differences between the optimized simulations and the measurements similar to Konovalov et al. (2014), except that possible uncertainties in emission factors were not explicitly taken into account in the Monte-Carlo experiment carried out in this study. Accordingly, the uncertainty in the estimates of F_α reported below reflects the uncertainty of the product of α and β^s (see Eq. 1), rather than the uncertainty in α alone.

In addition to the estimation of F_α by using ground based measurements, a similar procedure was used to derive estimates of F_α from satellite (MODIS) AOD measurements. The AOD-measurement-based values of F_α were used to obtain the "top-down" estimates of total BB aerosol emissions in the study region (see Sect. 3.4). In this case, the cost function J was formulated in the same way as in Konovalov et al. (2014):

$$J = \sum_{j=1}^{N_\mathrm{d}} \sum_{i=1}^{N_\mathrm{c}} \theta^{ij} \left(V_\mathrm{m}^{ij} - V_\mathrm{o}^{ij} - \Delta^{ij} \right)^2, \quad (6)$$

where V_m and V_o are the simulated and observed AOD values for each grid cell, i, and day, j, of our model domain, N_c is the total number of grid cells in the model domain, and θ^{ij} is the selection operator taken to be unity when relative contribution of fire

ACPD
15, 9107–9172, 2015

emissions to the simulated AOD exceeds 10 % and zero otherwise. Estimation of the bias, Δ, in our AOD simulations was the same as in Konovalov et al. (2014), except that here, instead of averaging the differences between the simulated and measured data within a "moving window" covering 15 consecutive days, the averaging was performed over the whole period of the study (because otherwise the number of data points with $\theta^{ij} = 0$ used for estimating of the bias in the situation considered in this study was too small).

2.7 Configuration and scenarios of simulations

To be able to efficiently isolate direct effects caused by changes in the aerosol scheme on the evolution of BB aerosol from any less direct effects involving possible interference of BB and other types of aerosol, our simulations included two stages. First, we carried out "background" simulations (labelled below as "BGR") without fire emissions but with all the other assumed aerosol sources (such as anthropogenic, dust and biogenic emissions). Taking into account that the VBS scheme had not ever been used and evaluated in simulations of aerosol evolution in Russia, we opted to simulate the background conditions by using the standard aerosol scheme. Second, the evolution of BB aerosol was simulated by running CHIMERE with fire emissions but without emissions from the other sources and with zero boundary conditions. Finally, concentrations of aerosol species were calculated as the sum of the outputs from these two model runs. Such a configuration of our simulations implies that the POA, as well as SOA and SVOCs originating from fires are not interacting with other types of aerosol. This may not be exactly true, but presently there are no available parameterizations which could be used to describe and evaluate such interactions. For the same reason, we disregarded formation of secondary inorganic aerosol from fire emissions. Taking into account that according to both our simulations and an independent analysis (see, e.g., Witte et al., 2011) air pollution levels over the study region in the period of intense fires were mostly determined by BB emissions, we expect that the impact of possible interaction of BB and other emissions on the results of this study is insignificant. Re-

ACPD
15, 9107–9172, 2015

sults of an additional control run, in which we took into account all the emission sources at once (and, consequently, all aerosol was assumed to be internally mixed) supported this expectation.

We considered several model scenarios with fire emissions, including the scenario in which BB aerosol evolution was simulated with the standard aerosol scheme (see Sect. 2.4.1) as well as five scenarios involving the VBS scheme. The scenario labels (used below both in the text and in the figures) and corresponding parameter settings are listed in Table 2. Specifically, along with the "standard" scenario (STN) we designed four "realistic" scenarios (from VBS-1 to VBS-4) in order to examine the sensitivity of our model results to possible uncertainties in the VBS scheme, while the "unrealistic" scenario VBS-5 was aimed at assessing the relative importance of the dilution process (under the assumption that there is no formation of SOA from oxidation of SVOC). In particular, we took into account that although Grieshop et al. (2009a) did not report a formal uncertainty range for the OH reaction rate k_{OH}, their results indicate that this rate could significantly vary in different experiments with different types of fuel; strong variability of k_{OH} is also indicated by a significant divergence of OA mass enhancements in the aging experiments by Hennigan et al. (2011) and Ortega et al. (2013). One of the scenarios was specified by taking into account the large uncertainty of the volatility distributions estimated by May et al. (2013). For example, the fraction of organic material in the highest volatility class ($C^* = 10^4\ \mu g\,m^{-3}$) considered by May et al. (2013) was estimated to range from 0.3 to 0.7 if the accommodation coefficient (γ) equals unity (see Table S4 in May et al., 2013). The two types of volatility distributions used in our simulations are specified in Table 3. Note that although the dilution experiment results by May et al. (2013) did not yield a unique value of the accommodation coefficient, we present here only the results obtained with the most probable (according to May et al., 2013) value of γ ($\gamma = 1.0$). An additional simulation was made with $\gamma = 0.1$, but since its results were found to be very similar to those obtained with $\gamma = 1.0$, they are not reported here.

ACPD
15, 9107–9172, 2015

3 Results

3.1 Near-surface concentrations

We focus our analysis on the air pollution events observed in the city of Kuopio (Finland) on 29 July and 8 August (Portin et al., 2012). Figure 2 demonstrates our model domains and shows "snapshots" of the simulated distributions of CO emitted by fires not only on these days but also on the preceding days (28 July and 7 August). Our simulations demonstrate that, in each episode, the smoke that appeared over Kuopio had been transported in the north-east direction from a region around Moscow, where the largest fires had occurred (Konovalov et al., 2011). As an illustration of sources of the smoke plumes, Fig. 2 also shows the spatial distributions of CO emissions from fires on 28 July and 7 August. We estimate that the age of smoke in the plumes passing over Kuopio was mostly in the range from 1 to 3 days. This estimate is in line with results of back-trajectory analyses (Portin et al., 2012). Note that CO behaved almost identically in all of the simulation scenarios in which the BB emissions were taken into account; therefore, for definiteness, the evolution of CO from fires is presented here only for the STN scenario (that is, with the scenario using the standard version of CHIMERE).

Figure 3 shows the evolution of CO in the Moscow region and in Kuopio according to both measurements and simulations. The simulations taking into account fire emissions were made with the optimal estimate of F_α (derived from CO measurements in Moscow and applied to emissions of all gaseous species in all of the simulations discussed below) of 1.88; the uncertainty of this estimate was evaluated in terms of the geometrical SD to be 1.14. Both the model and observations demonstrate episodes of very strong enhancements of CO concentration in both Moscow (mainly in early August) and in Kuopio (in the end of July and early August). The correlation of the simulated and observed time series is considerable at both locations ($r = 0.88$ in Moscow and $r = 0.76$ in Kuopio). Note that the optimization of just one parameter of our fire emission model (see Eqs. 1 and 2) could adjust the amplitude of CO variations in Moscow but could not insure the rather strong correlation between the simulations and measurements,

ACPD
15, 9107–9172, 2015

if our fire emission data were completely wrong. Most importantly, our simulations are capable of reproducing the major features of the observed CO evolution at a location about a thousand kilometers away from the source regions; in particular, the model and the measurements demonstrate a good agreement of "peak" CO concentrations on 29 July and 8 August. The differences between the simulated and observed CO concentrations in Kuopio can partly be due to the fact that this city was situated at the edge of the smoke plumes (see Fig. 2), where the concentration gradients were large and where the simulations were especially sensitive to any transport and emission errors. Note also that the rather high correlation obtained for the Kuopio site in the case of the BGR scenario ($r = 0.75$) reflects co-variation of the observations with a contribution of anthropogenic pollution transported from Russia to Finland to the CO level in Kuopio; however, the transport of anthropogenic CO (coinciding in space and time with the transport of CO from fires) can explain only a minor part of the observed CO variations. On the whole, the results shown in Fig. 3 indicate that both fire emissions and transport processes during the study period are simulated rather adequately by our modelling system, although not perfectly.

Time series of PM_{10} concentrations from simulations performed with the standard version of CHIMERE (that is, with the STN scenario) and with the VBS-2 scenario (which was found to best reproduce the high PM_{10} concentrations observed in Kuopio on 29 July and 8 August) are shown in Fig. 4 in comparison with corresponding measurement data. The optimal values of F_α applied in the simulations for these and the other scenarios to the emissions of all non-volatile and semi-volatile species were derived from PM_{10} measurements (as explained in Sect. 2.6) and are reported in Table 4.

In spite of the considerable differences between the representations of aerosol processes in the different aerosol schemes, simulations for the STN and all of the VBS scenarios demonstrate very similar performance when compared to the Moscow observations (see Fig. 4a and Table 4), mainly because these data have been used to adjust the emissions. However, major differences between the different simulation scenarios become evident when the simulated data are compared to the measurements

ACPD
15, 9107–9172, 2015

in Kuopio (see Fig. 4b and Table 5). Specifically, the VBS version of the model (for the VBS-2 scenario) predicts an about two times larger contribution of fire emissions to PM_{10} concentration on both 29 July and 8 August, and enables achieving much better agreement of the simulations with the measurements on these remarkable days than the standard version. The differences between the performance statistics calculated for the whole time series of the VBS and STN simulations are not quite unequivocal: on the one hand, the use of the VBS scheme instead of the standard scheme is associated with a decrease (from 7.3 to 6.7 $\mu g\,m^{-3}$) of the root mean square error (RMSE) and with improving agreement between the mean values of the observed and simulated PM_{10}; but, on the other hand, the VBS-2 scenario yields a slightly lower correlation coefficient (r = 0.88) than the STN scenario (r = 0.91). The decrease in the correlation coefficient is partly due to a strong overestimation of PM_{10} in the VBS simulation (similar to an overestimation of CO in the STN simulation) on 9 August.

Similar to the VBS-2 scenario, the other scenarios with the VBS scheme involving the POA oxidation parameterization by Grieshop et al. (2009a) yield considerably better agreement of simulations with measurements in Kuopio, compared to the STN scenario. The time series of PM_{10} concentrations from these and other scenarios considered (except for the scenario VBS-2 presented in Fig. 4b) are shown in Fig. 5. It is remarkable that the VBS-1 and VBS-4 scenarios yield almost indistinguishable results; that is, the sensitivity of our simulations to changes in the oxidation reaction rate is very small. This result indicates that atmospheric aerosol processing was sufficiently fast, so that those primary POA species that had been evaporated during their transport from the Moscow region to Finland were almost fully oxidized and absorbed by particles in any of the scenarios considered. Nonetheless, the scenario VBS-4 (which features the largest SVOC oxidation rate) yields slightly larger PM_{10} concentrations than the scenario VBS-1, as could be expected. It should be noted that the dependence of the OA concentration on the OH reaction rate or on the accommodation coefficient in the model is in general nonlinear, and the sensitivity of our simulations to changes of these parameters is small only in the limited range of the model parameter values. For exam-

ACPD
15, 9107–9172, 2015

ple, results for the VBS-5 scenario (with $k_{OH} = 0$) are quite different from those for the VBS-1 scenario in Kuopio. PM_{10} concentrations obtained for the VBS-3 scenario are significantly smaller compared to those calculated for the VBS-1 and VBS-4 scenarios. This is an expected result, taking into account that the parameterization by Jathar et al. (2014) assumes much smaller mass yields of the OPOA species than that by Grieshop et al. (2009a).

Note that the simulations presented in Fig. 5 were made using estimates of F_α adjusted independently for each scenario. This adjustment partly explains why the scenario "VBS-5" (under which a major fraction of initial particle emissions is expected to be irreversibly lost due to evaporation in the absence of SOA production from SVOCs) yields almost the same results as the scenario "STN". Indeed, the optimal F_α value for the VBS-5 scenario is 54 % larger than that for the STN scenario, and this fact indicates (taking into account the difference between the emission factors for POA and OC in accordance with Eq. 4) that about 46 % of primary POA species (mostly from the 6th and 7th volatility classes) already evaporated due to dilution (i.e., due to decrease in ambient C_{OA} levels) before they reached the monitoring sites in the Moscow regions. Further evaporation (mostly from the 5th volatility class) was relatively small and was partly offset by stronger production of SOA from oxidation of VOCs in the VBS scheme than in the standard aerosol scheme (as demonstrated below in Sect. 3.3). Unlike the VBS-5 scenario, the other VBS scenarios yield optimal F_α values that are very similar to that for the STN scenario. These estimates indicate that evaporation of POA species within the source region was effectively counterbalanced by SOA production.

To quantify the changes of aerosol concentrations relative to the concentration of CO (which can be regarded as a chemically passive tracer on the time scales considered in this study) in BB plumes, it is convenient to consider the normalized excess mixing ratio (NEMR) (similar, e.g. to Vakkari et al., 2014). In our case, NEMR can be defined as the ratio of ΔPM_{10} to ΔCO, where Δ denotes the "excess" concentration contributed by fires.

ACPD
15, 9107–9172, 2015

Figure 6 illustrates the spatial distributions of NEMR in the smoke plumes transported from Russia to Finland on 29 July and 8 August according to our simulations for the STN and VBS-2 scenarios. Evidently, the NEMR distributions obtained for these two scenarios are strikingly different. In particular, while NEMR calculated with the standard version of CHIMERE tends to decrease (apparently due to mainly aerosol deposition) as the smoke is transported away from the major fires that occurred south-east from Moscow (see Fig. 2e and f), the VBS version enables net production of aerosol during the same smoke transport events. Therefore, our simulations indicate a major role of oxidation processes, which dominate over evaporation of primary SVOCs due to smoke dilution and over dry deposition almost everywhere. As one of the spectacular manifestations of the fundamental differences between the representations of aerosol processes in the standard and VBS schemes, the NEMR values in the grid cell corresponding to Kuopio are more than two times larger in the VBS simulation than in the standard simulation. In general, the NEMR values are largest at the edges of the plumes, where the aerosol is likely to be more "aged" and more diluted. The increase of NEMR in the central (most dense) part of the plumes can be hampered by relatively slow evaporation of POA species and also by slowing-down of SVOC oxidation due to attenuation of photolysis rates by BB smoke (note a "valley" of NEMR local minimums in Fig. 6d along a direct (imaginary) line connecting Moscow and Kuopio; this "valley" coincides with the location of the thickest smoke (see Fig. 2d)).

To characterize the NEMR values over the whole study period, we evaluated the slope of a linear fit to a relationship between the ΔPM_{10} and ΔCO values on all days where the contribution of fires to CO concentration exceeded (according to our simulations) 10 %. Such "fitted" NEMR values (denoted below as $[\Delta PM_{10}/\Delta CO]_{fit}$) were calculated independently for the Moscow and Kuopio sites, both with the measurement and simulation data (see Fig. 7 and Tables 4 and 5).

Comparison of the $[\Delta PM_{10}/\Delta CO]_{fit}$ values calculated using measurement data reveals that $[\Delta PM_{10}/\Delta CO]_{fit}$ is almost two times larger in Kuopio ($0.13\,g\,g^{-1}$) than in Moscow ($0.069\,g\,g^{-1}$). We regard this fact (which was not noted in earlier publications)

ACPD
15, 9107–9172, 2015

as strong observational evidence of SOA formation in BB plumes during their transport from the Moscow region to Kuopio. In order to make sure that the major difference between the "observed" $[\Delta PM_{10}/\Delta CO]_{fit}$ values for Moscow and Kuopio is not an artefact of averaging of CO and PM_{10} measurements from 4 different monitoring stations in Moscow and/or a result of a technical failure of one of the monitors, we additionally evaluated $[\Delta PM_{10}/\Delta CO]_{fit}$ for each of the monitoring sites separately. The following values – 0.080, 0.056, 0.022, and 0.086 $g\,g^{-1}$ – were found with the data from the "Zelenograd", "MGU", "Pavlovskii Posad", and "Kozhuhovo" monitoring stations, respectively. All these values (in spite of their big differences, which probably reflect regional variability of ΔPM_{10} and ΔCO ratios due to varying emissions factors for different fires) are considerably smaller than the $[\Delta PM_{10}/\Delta CO]_{fit}$ value obtained from the measurements in the city of Kuopio.

In line with the results shown in Fig. 6a and c, the CHIMERE standard version (which yields little SOA in BB plumes) fails to explain the increase of NEMR in Kuopio by predicting a much smaller relative increase in the aerosol concentration: $[\Delta PM_{10}/\Delta CO]_{fit}$ is calculated to be only 10 % larger in Kuopio than in Moscow. Probably, this change mostly reflects the variability of the daily NEMR values. In contrast, the VBS-2 simulation reproduces the observed changes in the NEMR values almost perfectly. Using the VBS scheme with the other scenarios (except for the VBS-5 scenario) also results in a better agreement of the $[\Delta PM_{10}/\Delta CO]_{fit}$ values obtained from simulations and measurements (see Table 5).

3.2 Aerosol optical depth

Figure 8 presents the spatial distribution of AOD on 8 August 2010 according to simulations performed with the STN and VBS-2 scenarios in comparison with the corresponding MODIS measurement data. A very large BB plume reaching Kuopio is clearly visible both in the model and measurements data, although there are also considerable differences between measurement and simulations. Visually, the differences are largest between the measurement data and the simulations made with the STN sce-

ACPD
15, 9107–9172, 2015

nario: clearly, the standard model strongly underestimates AOD in many locations, including both Moscow and Kuopio. The differences between the measurements and the VBS-2 simulations are smaller, and much better agreement between them is evident compared to the results for the STN scenario. Interestingly, the VBS method gives significantly larger AOD than the standard method even in the source region, although the corresponding near-surface PM_{10} concentrations predicted with the both methods are very similar. In fact, we found that the VBS-2 simulation predicts a larger contribution of SOA to OA concentrations at higher altitudes (in the Moscow region) than to near–surface concentrations; this can be due to both a larger typical "age" of AO situated at higher altitudes and lower temperatures leading to more condensation of SVOCs.

Time series of daily AOD values averaged over the study region are shown in Fig. 9. Averaging the AOD data over the whole domain is expected to minimize the contribution of random errors in the simulations and measurements to the respective time series. Evidently, the standard simulation strongly underestimates AOD. The simulation with the VBS-2 scenario typically predicts a much larger (more than a factor of 2, on the average) contribution of BB aerosol to AOD, compared to the simulation with the STN scenario. Accordingly, the use of the VBS method instead of the standard one enables much better overall agreement of simulations with the measurements, although a negative bias in the simulated data is not completely eliminated. A part of this bias may, in principle, be due to uncertainty ($\sim 20\,\%$) in the estimate of the mass extinction efficiency employed in this study to convert the simulated aerosol mass column concentration into AOD (see also Sect. 2.3).

It should be kept in mind that not only our simulations are imperfect, but that the AOD measurement data that we use here for comparison can also contain considerable uncertainties. In particular, van Donkelaar et al. (2011) found that the relative error of the "operational" AOD retrievals at the 10 km × 10 km resolution in the Moscow region between 26 July and 20 August 2010 was on average about 20 %, and that a part of this error was due to incorrect identification of some aerosol as cloud. Although the uncertainties in the level 3 data product (at the $1^\circ \times 1^\circ$ resolution) used in this study

ACPD
15, 9107–9172, 2015

is likely to be smaller than those in the operational retrievals, spatial averaging could hardly diminish probable systematic uncertainties associated with the cloud screening algorithm. Based on the analysis by van Donkelaar et al. (2011), it seems safe to assume that those systematic uncertainties on average do not exceed 10 %; however, they may occasionally be much larger in grid cells where AOD is approaching a value of 5 (since the standard MODIS algorithm removes any retrieved AOD greater than this value).

3.3 Aerosol composition

Although our simulations based on a simple VBS scheme do not allow distinguishing between different chemical compounds contributing to OA matter, they still can provide some useful insight into the changes of aerosol composition caused by absorption/desorption and oxidation processes involving SVOC (that is, by the processes that are largely disregarded in the framework of the conventional approach to OA modelling). Figure 10 compares the speciation of BB aerosol according to our simulations made with the STN and VBS-2 scenarios. Specifically, we consider near-surface data from two model grid cells covering the city centers of Moscow and Kuopio. The Moscow and Kuopio data correspond to 18:00 UTC on 7 and 8 August, respectively: we expect that the differences between these data qualitatively reflect changes in the BB aerosol composition as a result of aerosol ageing during transport of BB plumes between the source and "recipient" regions considered.

Obviously, the results obtained with the standard and VBS schemes are profoundly different. In particular, while the STN simulation predicts that more than 90 % of BB aerosol composition is determined by POA species both in Moscow and in Kuopio, the VBS-2 scenario indicates a large contribution of secondary organic species (S-SOA) originating from oxidation of SVOCs. As expected, the fraction of S-SOA species is much larger in Kuopio (71 %) than in Moscow (38 %), with the POA fraction shrinking from 49 % in Moscow to merely 12 % in Kuopio. Note that a considerable S-SOA fraction in Moscow confirms that oxidation processes were rapid enough to already trans-

ACPD
15, 9107–9172, 2015

form the composition of BB aerosol on its way (typically having taken several hours) from the fire spots to Moscow.

Compared to the standard scheme, the VBS scheme yields also a larger fraction of SOA (V-SOA) formed from oxidation of volatile (traditional) precursors, but the contribution of V-SOA still remains minor even in the aged plumes. Both scenarios predict that the black carbon (BC) fraction is, expectedly, also small at both locations and does not exceed 5 %. Our results for Moscow are compatible with the average OC/BC ratio of 14.2 observed there by Popovicheva et al. (2014) on smoky days in August 2010 (assuming that the ratio of POM to OC was about 2, this observation indicates that the mass fraction of BC was on average about 3.5 %). Interestingly, the BC fraction in Kuopio is almost 2 times less in the VBS simulation than in the standard model run. This is a result of increasing the total mass of aerosol particles due to absorption of oxidized material. Data of BC measurements in Kuopio were available only from the Puijo tower atmospheric measurement station (Leskinen et al., 2009; Portin et al., 2012), which unfortunately did not provide simultaneous accurate measurements of PM_{10} or OC. However, if we assume that the contribution of BB aerosol to PM_{10} on the "smoky" days (29 July and 8 August) at the Puijo site was the same as that to PM_{10} at the Maaherrankatu site, we can estimate (using the data from Table 1 in Portin et al., 2012) that the mass fraction of BC aerosol was about 2 %. Obviously, using such an "approximate" estimate does not enable us to make any firm conclusion about the relative accuracy of our VBS-2 or STN simulations with regard to the BC fraction, but nonetheless it indicates that the BC fraction in BB aerosol in Kuopio could be lower than that predicted by the standard model.

3.4 Top-down estimates of BB aerosol emissions

Obtaining top-down estimates (that is, estimates constrained by atmospheric measurements) of emissions of aerosols (as well as gaseous species) by using the inverse modelling approach (see, e.g., Enting, 2002; Zhang et al., 2005; Dubovik et al., 2008; Huneeus et al., 2012; Xu et al., 2013) is aimed at validation and improving "bottom-

ACPD
15, 9107–9172, 2015

up" emission inventories and advancing our general knowledge of the emission processes. As noted in the introduction, the models employed in inverse modelling studies have conventionally simulated BB aerosol under the assumption that it consists of non-volatile material. Here we examined, in particular, whether or not top-down estimates of BB emissions could change significantly if this assumption was relaxed in accordance with the VBS approach to OA modelling.

We obtained top-down estimates of total emissions of aerosol from fires in the study region during the period from 1 July to 31 August 2010 by using the MODIS AOD measurements and the correction factor (F_α) values estimated for the period covered by our simulations (from 15 July to 20 August). The F_α estimates are applied to the extended period, taking into account that fire emissions in the first half of July and the second half of August were relatively very small, in order to compare our emission estimates with available monthly data of bottom-up inventories. Our emission estimates, along with the corresponding estimates of the correction factor F_α for the same modelling scenarios as those discussed above (except for the estimates for the "unrealistic" scenario "VBS-5"), are presented in Fig. 11. The emissions estimates are shown in comparison with the data from the bottom-up fire emission inventories, such as GFED3.1 and GFASv1.0, for emissions of total particulate matter (TPM), while the estimates of F_α derived from satellite measurements are presented along with the corresponding estimates obtained from ground-based measurements (see also Table 4). The estimates for the scenario VBS-5 are omitted from these figures, because they turn out to be much larger (as could be expected) than those for all the other scenarios and are clearly unrealistic (in particular, the total aerosol emissions were 1.8 Tg according to the VBS-5 scenario, compared to 1.3 Tg for the STN scenario). The much larger estimate for the VBS-5 scenario (relative to the estimates for the both STN scenario and the other VBS scenarios) is indicative of the major roles of both SOA formation and dilution of POA in the study region during the period of intense fires. Note that the uncertainties of the different estimates of the top-down emissions and the correction factors are not statistically independent. The emission estimates for the VBS scenarios

ACPD
15, 9107–9172, 2015

are reported assuming the ambient level of OA concentration (C_{OA}) during the emission factor measurements to be 10 mg m^{-3} (see Sect. 2.4.2); under this assumption, the total POA emissions are about 20 % larger. Optimization of F_α is expected to compensate possible uncertainties in the POA emission factors. Note again that the experimental data for the OA emission factors can depend (as argued, e.g., by Robinson et al., 2007) on C_{OA} and ambient temperature, which are unfortunately not reported in the literature together with the emission factor estimates.

It is remarkable that (1) the BB aerosol emission estimate obtained using the standard model (1.3 Tg TPM) is about 60 % larger than the corresponding estimate based on using the VBS approach with the VBS-2 scenario (0.8 Tg TPM), (2) the estimates for the scenarios "VBS-1" and "VBS-4" are also considerably smaller than the estimate for the STN scenario, (3) all estimates based on using the VBS approach (except for the estimate for the unrealistic VBS-5 scenario) show better agreement with both the GFASv1.0 and GFED3.1 data than the estimate for the STN scenario. Another important result is that the optimal estimate of F_α (and the corresponding top-down emission estimates) derived from the AOD measurements for the VBS-2 scenario is consistent (within the range uncertainty) with the corresponding estimate derived from local near-surface monitoring data, while this is obviously not the case with the estimate obtained by using the standard approach. The inconsistency of the estimates based on the independent data means that they fail to pass the cross-validation, and is indicative of major deficiencies of simulations based on the standard approach. On the other hand, the fact that the estimates of F_α derived from satellite and ground-based measurements at least with the "best" VBS scenario are consistent provides strong evidence in favor of the reliability of our top-down emission estimates obtained with the VBS approach. Regarding the remaining differences between our emission estimates and the corresponding data of the GFED3.1 inventory, it can be noted that there is evidence (e.g., Fokeeva et al., 2011; Konovalov et al., 2011; Krol et al., 2013) that the GFED3.1 inventory strongly underestimated the CO emissions from the 2010 Russian fires; it seems

ACPD
15, 9107–9172, 2015

thus reasonable to expect that the TPM emissions were also underestimated by this inventory.

4 Summary and concluding remarks

In this study, we used the volatility basis set (VBS) approach to organic aerosol (OA) modelling to simulate the mesoscale evolution of aerosol from open biomass burning for the case of the mega-fire event that occurred in Russia in summer 2010. We modified the VBS scheme in the CHIMERE chemistry transport model by using data from laboratory experiments aimed at studying gas-particle partitioning and oxidation processes in the mixtures of gases and aerosols emitted from biomass burning (BB). Unlike the VBS approach, the "conventional" OA modeling approach used in the standard version of CHIMERE disregards the volatility of primary OA species and the formation of secondary organic aerosol by oxidation of semi-volatile precursors. Several simulations scenarios were considered to test the sensitivity of the model output data to possible uncertainties in the parameters of the VBS scheme and to evaluate the relative role of dilution and oxidation processes in the evolution of aerosol in BB plumes. Emissions of gases and particles from fires were modelled using fire radiative power (FRP) data from satellite (MODIS) measurements, and were constrained by CO and PM_{10} air pollution monitoring data in the Moscow region.

The results of simulations made with the VBS scheme are compared with corresponding results obtained with the standard OA scheme in CHIMERE and with data from ground-based and satellite measurements. In particular, we evaluated our simulations with respect to the normalized excess mixing ratio (NEMR) of BB aerosol (defined as the ratio of enhancements caused by fires in PM_{10} and CO concentrations) by using measurements at an air pollution monitoring site in the city of Kuopio, Finland (situated about 1000 km north-west from Moscow). While the standard simulations were found to strongly underestimate the observed NEMR in Kuopio (which turned out to be about two times larger there than in Moscow, thus indicating the gain of BB aerosol

ACPD
15, 9107–9172, 2015

mass during transport from Russia to Finland), the simulations based on the VBS approach proved to be in a good agreement with the measurements. Similar results were obtained when evaluating our simulations against satellite AOD measurements. In particular, the use of the VBS approach enabled reducing RMSE of simulations by almost a factor of two relative the simulations based on the "conventional" approach.

It should be emphasized that our numerical experiments with the VBS scheme were neither intended nor allowed us to estimate the real values of the parameters of the processes considered. Indeed, our VBS scheme provides only a very simplistic representation of the complex processes involving absorption/desorption and oxidation of organic material. For example, Donahue et al. (2012) argue that assuming a two-dimensional volatility-oxidation space (2-D-VBS) enables constraining the average organic properties more tightly than the more conventional one-dimensional scheme used in this study. An even much more complex (and potentially realistic) OA evolution scheme could involve explicit characterization of chemical and physical properties of different organic species (Aumont et al., 2005). A general problem arising with more complex schemes is the lack of sufficient laboratory or ambient measurement data needed to constrain all the parameters. On the other hand, there is always the possibility that a simplistic scheme may demonstrate good performance for a wrong reason; for example, when optimization of its parameters compensates some systematic model errors. In our case, systematic model errors may be associated, in particular, with disregarding the fragmentation process (splitting of C-C bonds, which tends to increase volatility) and a simplified representation of the functionalization processes (which tend to decrease volatility); a potentially important role of these processes was discussed in detail, e.g., by Murphy et al. (2012). Our model also disregards formation of new OA particles (i.e., the nucleation process), which may be important at least during the initial hours of the atmospheric processing of BB smoke (e.g., Vakkari et al., 2014). Nonetheless, our results provide strong evidence that the VBS method applied in this study to a special case of modeling aerosol originating from wildfires is indeed superior to the "conventional" method.

ACPD
15, 9107–9172, 2015

Important implications of using the VBS instead of the "conventional" approach for modeling the evolution of BB aerosol include, in particular, major changes in the composition of the aerosol particles. Our results show that the ageing of BB aerosol is associated with replacement of primary organic aerosol (POA) species by secondary organic aerosol (SOA) species, formed mostly from oxidation of semi-volatile organic compounds (SVOC). Specifically, according to our VBS simulations, SOA contributed about 90 % to BB aerosol in Kuopio during an air pollution event on 8 August 2010. Oxygenated organics are likely to contain light-absorptive brown carbon (Saleh et al., 2013), are known to be more hygroscopic (Jimenez et al., 2009) and are expected to have a larger health impact, when inhaled as particles (Stevanovic et al., 2013), than primary organics. Therefore, BB aerosol ageing (which obviously cannot be described adequately with the "conventional" approach) should be taken into account in climate models where the absorptivity and hygroscopicity of aerosol (providing cloud condensation nuclei) are important parameters (e.g., Andreae and Ramanathan, 2013; Andreae and Rosenfeld, 2008; Pöschl et al., 2009) as well as in air pollution models.

Finally, we found that the replacement of the standard aerosol model in CHIMERE by the VBS scheme had a considerable impact on the top-down BB emission estimates derived from satellite AOD measurements by means of inverse modeling. Specifically, the total BB aerosol emissions from the 2010 Russian fires in the region and period considered in this study are estimated to be about 60 % larger with the "conventional" method than with the VBS scheme. Moreover, it was found that while both satellite and ground based measurements enabled consistent constraints to aerosol emissions from the 2010 Russian fires when CHIMERE employs the VBS scheme, this was not the case when the standard aerosol scheme was used.

Future studies of BB aerosol evolution, combining modeling with laboratory and field measurements, should provide stronger constraints to the parameters of the OA transformation processes addressed in the framework of the VBS approach, and enable further development of the VBS approach for the particular case of OA originating from open biomass burning. Further efforts are also needed for achieving better under-

ACPD
15, 9107–9172, 2015

standing of possible differences between the ageing of BB aerosol from fires in different regions and climate zones and addressing these differences in chemistry transport and climate models.

Acknowledgements. This study was supported by the Russian Foundation for Basic Research (grants No. 14-05-00481 and 15-45-02516) and the Russian Academy of Sciences in the framework of the Programme for Basic Research "Electrodynamics of atmosphere; Electrical Processes, Radiophysical Methods of Research". The authors are grateful to E. G. Semutnikova for providing the Mosecomonitoring data. The authors are also grateful to the City of Kuopio for the air quality data. T. Mielonen's work was supported by Academy of Finland Center of Excellence Program (decision 272041).

References

Ahmadov, R., McKeen, S. A., Robinson, A. L., Bahreini, R., Middlebrook, A. M., de Gouw, J. A., Meagher, J., Hsie, E.-Y., Edgerton, E., Shaw, S., and Trainer, M.: A volatility basis set model for summertime secondary organic aerosols over the eastern United States in 2006, J. Geophys. Res., 117, D06301, doi:10.1029/2011JD016831, 2012. 9112

Akagi, S. K., Yokelson, R. J., Wiedinmyer, C., Alvarado, M. J., Reid, J. S., Karl, T., Crounse, J. D., and Wennberg, P. O.: Emission factors for open and domestic biomass burning for use in atmospheric models, Atmos. Chem. Phys., 11, 4039–4072, doi:10.5194/acp-11-4039-2011, 2011. 9121

Akagi, S. K., Craven, J. S., Taylor, J. W., McMeeking, G. R., Yokelson, R. J., Burling, I. R., Urbanski, S. P., Wold, C. E., Seinfeld, J. H., Coe, H., Alvarado, M. J., and Weise, D. R.: Evolution of trace gases and particles emitted by a chaparral fire in California, Atmos. Chem. Phys., 12, 1397–1421, doi:10.5194/acp-12-1397-2012, 2012. 9112

Alves, C., Vicente, A., Nunes, T., Gonçalvesa, C., Fernandesa, A. P., Mirantea, F., Tarelhoa, L., de la Campab, A. M. S., Querolc, X., Caseiroa, A., Monteiroa, C., Evtyuginaa, M., and Pioa, C.: Summer 2009 wildfires in Portugal: emission of trace gases and aerosol composition, Atmos. Environ., 45, 641–649, 2011. 9119, 9120

Andreae, M. O. and Merlet, P.: Emission of trace gases and aerosols from biomass burning, Global Biogeochem. Cy., 15, 955–966, doi:10.1029/2000GB001382, 2001. 9110, 9118, 9124

ACPD
15, 9107–9172, 2015

Andreae, M. O. and Ramanathan, V.: Climate's dark forcings, Science, 340, 280–281, doi:10.1126/science.1235731, 2013. 9110, 9143

Andreae, M. O. and Rosenfeld, D.: Aerosol–cloud–precipitation interactions. Part 1. The nature and sources of cloud-active aerosols, Earth-Sci. Rev., 89, 13–41, 2008. 9143

Aumont, B., Szopa, S., and Madronich, S.: Modelling the evolution of organic carbon during its gas-phase tropospheric oxidation: development of an explicit model based on a self generating approach, Atmos. Chem. Phys., 5, 2497–2517, doi:10.5194/acp-5-2497-2005, 2005. 9142

Barriopedro, D., Fischer, E. M., Luterbacher, J., Trigo, R. M., and García-Herrera, R.: The hot summer of 2010: redrawing the temperature record map of Europe, Science, 332, 220–224, 2011. 9112

Bergström, R., Denier van der Gon, H. A. C., Prévôt, A. S. H., Yttri, K. E., and Simpson, D.: Modelling of organic aerosols over Europe (2002–2007) using a volatility basis set (VBS) framework: application of different assumptions regarding the formation of secondary organic aerosol, Atmos. Chem. Phys., 12, 8499–8527, doi:10.5194/acp-12-8499-2012, 2012. 9112

Bertschi, I. T. and Jaffe, D. A.: Long-range transport of ozone, carbon monoxide, and aerosols in the NE Pacific troposphere during the summer of 2003: observations of smoke plumes from Asian boreal fires, J. Geophys. Res., 110, D05303, doi:10.1029/2004JD005135, 2005. 9110

Bessagnet, B., Menut, L., Curci, G., Hodzic, A., Guillaume, B., Liousse, C., Moukhtar, S., Pun, B., Seigneur, C., and Schulz, M.: Regional modeling of carbonaceous aerosols over Europe – focus on secondary organic aerosols, J. Atmos. Chem., 61, 175–202, 2009. 9120

Bond, T. C., Doherty, S. J., Fahey, D. W., Forster, P. M., Berntsen, T., DeAngelo, B. J., Flanner, M. G., Ghan, S., Kärcher, B., Koch, D., Kinne, S., Kondo, Y., Quinn, P. K., Sarofim, M. C., Schultz, M. G., Schulz, M., Venkataraman, C., Zhang, H., Zhang, S., Bellouin, N., Guttikunda, S. K., Hopke, P. K., Jacobson, M. Z., Kaiser, J. W., Klimont, Z., Lohmann, U., Schwarz, J. P., Shindell, D., Storelvmo, T., Warren, S. G., and Zender, C. S.: Bounding the role of black carbon in the climate system: a scientific assessment, J. Geophys. Res.-Atmos., 118, 5380–5552, doi:10.1002/jgrd.50171, 2013. 9110

Bowman, F. M., Odum, J. R., Seinfeld, J. H., and Pandis, S. N.: Mathematical model for gas-particle partitioning of secondary organic aerosols, Atmos. Environ., 31, 3921–3931, 1997. 9122

ACPD
15, 9107–9172, 2015

Carter, W. P. L.: Development of the SAPRC-07 chemical mechanism, Atmos. Environ., 44, 5324–5335, doi:10.1016/j.atmosenv.2010.01.026, 2010. 9114

Chacon-Madrid, H. J. and Donahue, N. M.: Fragmentation vs. functionalization: chemical aging and organic aerosol formation, Atmos. Chem. Phys., 11, 10553–10563, doi:10.5194/acp-11-10553-2011, 2011. 9124

Chakrabarty, R. K., Moosmüller, H., Chen, L.-W. A., Lewis, K., Arnott, W. P., Mazzoleni, C., Dubey, M. K., Wold, C. E., Hao, W. M., and Kreidenweis, S. M.: Brown carbon in tar balls from smoldering biomass combustion, Atmos. Chem. Phys., 10, 6363–6370, doi:10.5194/acp-10-6363-2010, 2010. 9110

Derognat, C., Beekmann, M., Baeumle, M., Martin, D., and Schmidt, H.: Effect of biogenic volatile organic compound emissions on tropospheric chemistry during the Atmospheric Pollution Over the Paris Area (ESQUIF) campaign in the Ile-de-France region, J. Geophys. Res.-Atmos., 108, 8560, doi:10.1029/2001JD001421, 2003. 9114

Donahue, N. M., Robinson, A. L., Stanier, C. O., and Pandis, S. N.: Coupled partitioning, dilution, and chemical aging of semivolatile organics, Environ. Sci. Technol., 40, 2635–2643, doi:10.1021/es052297c, 2006. 9111, 9112, 9119

Donahue, N. M., Kroll, J. H., Pandis, S. N., and Robinson, A. L.: A two-dimensional volatility basis set – Part 2: Diagnostics of organic-aerosol evolution, Atmos. Chem. Phys., 12, 615–634, doi:10.5194/acp-12-615-2012, 2012. 9111, 9124, 9142

Dubovik, O., Lapyonok, T., Kaufman, Y. J., Chin, M., Ginoux, P., Kahn, R. A., and Sinyuk, A.: Retrieving global aerosol sources from satellites using inverse modeling, Atmos. Chem. Phys., 8, 209–250, doi:10.5194/acp-8-209-2008, 2008. 9138

Elansky, N. F., Mokhov, I. I., Belikov, I. B., Berezina, E. V., Elokhov, A. S., Ivanov, V. A., Pankratova, N. V., Postylyakov, O. V., Safronov, A. N., Skorokhod, A. I., and Shumskii, R. A.: Gaseous admixtures in the atmosphere over Moscow during the 2010 summer, Izv. Atmos. Ocean. Phy.+, 47, 672–681, doi:10.1134/S000143381106003X, 2011. 9113

EMEP/CEIP: Present state of emissions as used in EMEP models, available at: http://www.ceip.at/webdab_emepdatabase/emissions_emepmodels/ (last access: 25 March 2015), 2014. 9115

Engling, G., He, J., Betha, R., and Balasubramanian, R.: Assessing the regional impact of indonesian biomass burning emissions based on organic molecular tracers and chemical mass balance modeling, Atmos. Chem. Phys., 14, 8043–8054, doi:10.5194/acp-14-8043-2014, 2014. 9110

ACPD
15, 9107–9172, 2015

Enting, I. G.: Inverse Problems in Atmospheric Constituents Transport, Cambridge University Press, Cambridge, 2002. 9138
Farina, S. C., Adams, P. J., and Pandis, S. N.: Modeling global secondary organic aerosol formation and processing with the volatility basis set: implications for anthropogenic secondary organic aerosol, J. Geophys. Res., 115, D09202, doi:10.1029/2009JD013046, 2010. 9112
Fiebig, M., Stohl, A., Wendisch, M., Eckhardt, S., and Petzold, A.: Dependence of solar radiative forcing of forest fire aerosol on ageing and state of mixture, Atmos. Chem. Phys., 3, 881–891, doi:10.5194/acp-3-881-2003, 2003. 9120
Fokeeva, E. V., Safronov, A. N., Rakitin, V. S., Yurganov, L. N., Grechko, E. I., and Shumskii, R. A.: Investigation of the 2010 July–August fires impact on carbon monoxide atmospheric pollution in Moscow and its outskirts, estimating of emissions, Izv. Atmos. Ocean. Phy.+, 47, 682–698, 2011. 9140
Folberth, G. A., Hauglustaine, D. A., Lathière, J., and Brocheton, F.: Interactive chemistry in the Laboratoire de Météorologie Dynamique general circulation model: model description and impact analysis of biogenic hydrocarbons on tropospheric chemistry, Atmos. Chem. Phys., 6, 2273–2319, doi:10.5194/acp-6-2273-2006, 2006. 9115
Golitsyn, G. S., Gorchakov, G. I., Grechko, E. I., Semoutnikova, E. G., Rakitin, V. S., Fokeeva, E. V., Karpov, A. V., Kurbatov, G. A., Baikova, E. S., and Safrygina, T. P.: Extreme carbon monoxide pollution of the atmospheric boundary layer in Moscow region in the summer of 2010, Dokl. Earth Sci., 441, 1666–1672, 2012. 9113
Goodrick, S. L., Achtemeier, G. L., Larkin, N. K., Liu, Y., and Strand. T. M.: Modelling smoke transport from wildland fires: a review, Int. J. Wildland Fire, 22, 83–94, doi:10.1071/WF11116, 2012. 9110
Grieshop, A. P., Logue, J. M., Donahue, N. M., and Robinson, A. L.: Laboratory investigation of photochemical oxidation of organic aerosol from wood fires 1: measurement and simulation of organic aerosol evolution, Atmos. Chem. Phys., 9, 1263–1277, doi:10.5194/acp-9-1263-2009, 2009a. 9111, 9123, 9124, 9129, 9132, 9133, 9158
Grieshop, A. P., Miracolo, M. A., Donahue, N. M., and Robinson, A. L.: Constraining the volatility distribution and gas-particle partitioning of combustion aerosols using isothermal dilution and thermodenuder measurements, Environ. Sci. Technol., 43, 4750–4756, doi:10.1021/es8032378, 2009b. 9111
Guenther, A., Karl, T., Harley, P., Wiedinmyer, C., Palmer, P. I., and Geron, C.: Estimates of global terrestrial isoprene emissions using MEGAN (Model of Emissions of Gases and

ACPD
15, 9107–9172, 2015

Aerosols from Nature), Atmos. Chem. Phys., 6, 3181–3210, doi:10.5194/acp-6-3181-2006, 2006. 9115
Heil, A. and Goldammer, J. G.: Smoke-haze pollution: a review of the 1997 episode in Southeast Asia, Reg. Environ. Change, 2, 24–37, doi:10.1007/s101130100021, 2001. 9110
Hennigan, C. J., Miracolo, M. A., Engelhart, G. J., May, A. A., Presto, A. A., Lee, T., Sullivan, A. P., McMeeking, G. R., Coe, H., Wold, C. E., Hao, W.-M., Gilman, J. B., Kuster, W. C., de Gouw, J., Schichtel, B. A., Collett Jr., J. L., Kreidenweis, S. M., and Robinson, A. L.: Chemical and physical transformations of organic aerosol from the photo-oxidation of open biomass burning emissions in an environmental chamber, Atmos. Chem. Phys., 11, 7669–7686, doi:10.5194/acp-11-7669-2011, 2011. 9111, 9123, 9124, 9129
Hennigan, C. J., Westervelt, D. M., Riipinen, I., Engelhart, G. J., Lee, T., Collett, J. L., Pandis, S. N., Adams, P. J., and Robinson, A. L.: New particle formation and growth in biomass burning plumes: an important source of cloud condensation nuclei, Geophys. Res. Lett., 39, L09805, doi:10.1029/2012GL050930, 2012. 9111
Hobbs, P. V., Sinha, P., Yokelson, R. J., Christian, T. J., Blake, D. R., Gao, S., Kirchstetter, T. W., Novakov, T., and Pilewskie, P.: Evolution of gases and particles from a savanna fire in South Africa, J. Geophys. Res., 108, D13, doi:10.1029/2002JD002352, 2003. 9112
Hodzic, A., Madronich, S., Bohn, B., Massie, S., Menut, L., and Wiedinmyer, C.: Wildfire particulate matter in Europe during summer 2003: meso-scale modeling of smoke emissions, transport and radiative effects, Atmos. Chem. Phys., 7, 4043–4064, doi:10.5194/acp-7-4043-2007, 2007. 9114
Hodzic, A., Jimenez, J. L., Madronich, S., Aiken, A. C., Bessagnet, B., Curci, G., Fast, J., Lamarque, J.-F., Onasch, T. B., Roux, G., Schauer, J. J., Stone, E. A., and Ulbrich, I. M.: Modeling organic aerosols during MILAGRO: importance of biogenic secondary organic aerosols, Atmos. Chem. Phys., 9, 6949–6981, doi:10.5194/acp-9-6949-2009, 2009. 9120
Hodzic, A., Jimenez, J. L., Madronich, S., Canagaratna, M. R., DeCarlo, P. F., Kleinman, L., and Fast, J.: Modeling organic aerosols in a megacity: potential contribution of semi-volatile and intermediate volatility primary organic compounds to secondary organic aerosol formation, Atmos. Chem. Phys., 10, 5491–5514, doi:10.5194/acp-10-5491-2010, 2010. 9112, 9119
Huffman, J. A., Docherty, K. S., Mohr, C., Cubison, M. J., Ulbrich, I. M., Ziemann, P. J., Onasch, T. B., and Jimenez, J. L.: Chemically resolved volatility measurements of organic aerosol from different sources, Environ. Sci. Technol., 43, 5351–5357, doi:10.1021/Es803539d, 2009. 9111

ACPD
15, 9107–9172, 2015

Huijnen, V., Flemming, J., Kaiser, J. W., Inness, A., Leitão, J., Heil, A., Eskes, H. J., Schultz, M. G., Benedetti, A., Hadji-Lazaro, J., Dufour, G., and Eremenko, M.: Hindcast experiments of tropospheric composition during the summer 2010 fires over western Russia, Atmos. Chem. Phys., 12, 4341–4364, doi:10.5194/acp-12-4341-2012, 2012. 9113

Huneeus, N., Chevallier, F., and Boucher, O.: Estimating aerosol emissions by assimilating observed aerosol optical depth in a global aerosol model, Atmos. Chem. Phys., 12, 4585–4606, doi:10.5194/acp-12-4585-2012, 2012. 9138

Ichoku, C. and Kaufman, J. Y.: A method to derive smoke emission rates from MODIS fire radiative energy measurements, IEEE T. Geosci. Remote, 43, 2636–2649, 2005. 9114, 9115, 9117

IPCC: Summary for policymakers, in: Climate Change 2013: The Physical Science Basis. Contribution of Working Group I to the Fifth Assessment Report of the Intergovernmental Panel on Climate Change, edited by: Stocker, T. F., Qin, D., Plattner, G.-K., Tignor, M., Allen, S. K., Boschung, J., Nauels, A., Xia, Y., Bex, V., and Midgley, P. M., Cambridge University Press, Cambridge, UK, New York, NY, USA, 3–29, 2013. 9110

Jacobson, M. Z.: Strong radiative heating due to the mixing state of black carbon in atmospheric aerosols, Nature, 409, 695–697, doi:10.1038/35055518, 2001. 9110

Janjic, Z. I.: The step-mountain coordinate: physical package, Mon. Weather Rev., 118, 1429–1443, 1990. 9116

Janjic, Z. I.: The step-mountain eta coordinate model: further developments of the convection, viscous sublayer and turbulence closure schemes, Mon. Weather Rev., 122, 927–945, 1994. 9116

Jathar, S. H., Gordon, T. D., Hennigan, C. J., Pye, H. O. T., Pouliot, G., Adams, P. J., Donahue, N. M., and Robinson, A. L.: Unspeciated organic emissions from combustion sources and their influence on the secondary organic aerosol budget in the United States, P. Natl. Acad. Sci. USA, 111, 10473–10478, doi:10.1073/pnas.1323740111, 2014. 9123, 9124, 9133, 9158

Jimenez, J. L., Canagaratna, M. R., Donahue, N. M., Prevot, A. S. H., Zhang, Q., Kroll, J. H., DeCarlo, P. F., Allan, J. D., Coe, H., Ng, N. L., Aiken, A. C., Docherty, K. S., Ulbrich, I. M., Grieshop, A. P., Robinson, A. L., Duplissy, J., Smith, J. D., Wilson, K. R., Lanz, V. A., Hueglin, C., Sun, Y. L., Tian, J., Laaksonen, A., Raatikainen, T., Rautiainen, J., Vaattovaara, P., Ehn, M., Kulmala, M., Tomlinson, J. M., Collins, D. R., Cubison, M. J., Dunlea, E. J., Huffman, J. A., Onasch, T. B., Alfarra, M. R., Williams, P. I., Bower, K., Kondo, Y., Schnei-

ACPD
15, 9107–9172, 2015

der, J., Drewnick, F., Borrmann, S., Weimer, S., Demerjian, K., Salcedo, D., Cottrell, L., Griffin, R., Takami, A., Miyoshi, T., Hatakeyama, S., Shimono, A., Sun, J. Y., Zhang, Y. M., Dzepina, K., Kimmel, J. R., Sueper, D., Jayne, J. T., Herndon, S. C., Trimborn, A. M., Williams, L. R., Wood, E. C., Middlebrook, A. M., Kolb, C. E., Baltensperger, U., and Worsnop, D. R.: Evolution of Organic Aerosols in the Atmosphere, Science, 326, 1525–1529, doi:10.1126/science.1180353, 2009. 9143

Kaiser, J. W., Heil, A., Andreae, M. O., Benedetti, A., Chubarova, N., Jones, L., Morcrette, J.-J., Razinger, M., Schultz, M. G., Suttie, M., and van der Werf, G. R.: Biomass burning emissions estimated with a global fire assimilation system based on observed fire radiative power, Biogeosciences, 9, 527–554, doi:10.5194/bg-9-527-2012, 2012. 9111, 9117

Keil, A. and Haywood, J. M.: Solar radiative forcing by biomass burning aerosol particles during SAFARI 2000: a case study based on measured aerosol and cloud properties, J. Geophys. Res., 108, D13, doi:10.1029/2002JD002315, 2003. 9110

Kiehl, J. T.: Twentieth century climate model response and climate sensitivity, Geophys. Res. Lett., 34, L22710, doi:10.1029/2007GL031383, 2007. 9110

Konovalov, I. B., Beekmann, M., Kuznetsova, I. N., Yurova, A., and Zvyagintsev, A. M.: Atmospheric impacts of the 2010 Russian wildfires: integrating modelling and measurements of an extreme air pollution episode in the Moscow region, Atmos. Chem. Phys., 11, 10031–10056, doi:10.5194/acp-11-10031-2011, 2011. 9110, 9111, 9113, 9114, 9115, 9117, 9118, 9119, 9125, 9126, 9127, 9130, 9140

Konovalov, I. B., Beekmann, M., D'Anna, B., and George, C.: Significant light induced ozone loss on biomass burning aerosol: evidence from chemistry-transport modeling based on new laboratory studies, Geophys. Res. Lett., 39, L17807, doi:10.1029/2012GL052432, 2012. 9114

Konovalov, I. B., Berezin, E. V., Ciais, P., Broquet, G., Beekmann, M., Hadji-Lazaro, J., Clerbaux, C., Andreae, M. O., Kaiser, J. W., and Schulze, E.-D.: Constraining CO_2 emissions from open biomass burning by satellite observations of co-emitted species: a method and its application to wildfires in Siberia, Atmos. Chem. Phys., 14, 10383–10410, doi:10.5194/acp-14-10383-2014, 2014. 9111, 9114, 9115, 9117, 9118, 9119, 9127, 9128

Krol, M., Peters, W., Hooghiemstra, P., George, M., Clerbaux, C., Hurtmans, D., McInerney, D., Sedano, F., Bergamaschi, P., El Hajj, M., Kaiser, J. W., Fisher, D., Yershov, V., and Muller, J.-P.: How much CO was emitted by the 2010 fires around Moscow?, Atmos. Chem. Phys., 13, 4737–4747, doi:10.5194/acp-13-4737-2013, 2013. 9113, 9140

ACPD
15, 9107–9172, 2015

Kroll, J. H., Ng, N. L., Murphy, S. M., Flagan, R. C., and Seinfeld, J. H.: Secondary organic aerosol formation from isoprene photooxidation, Environ. Sci. Technol., 40, 1869–1877, doi:10.1021/es0524301, 2006. 9120

Lane, T. E., Donahue, N. M., and Pandis, S. N.: Simulating secondary organic aerosol formation using the volatility basis-set approach in a chemical transport model, Atmos. Environ., 42, 7439–7451, 2008. 9112, 9119

Langmann, B., Duncan, B., Textor, C., Trentmann, J., and van der Werf, G. R.: Vegetation fire emissions and their impact on air pollution and climate, Atmos. Environ., 43, 107–116, doi:10.1016/j.atmosenv.2008.09.047, 2009. 9110

Leskinen, A., Portin, H., Komppula, M., Miettinen, P., Arola, A., Lihavainen, H., Hatakka, J., Laaksonen, A., and Lehtinen, K. E. J.: Overview of the research activities and results at Puijo semi-urban measurement station, Boreal Environ. Res., 14, 576–590, 2009. 9138

Levy, R. C., Remer, L. A., Kleidman, R. G., Mattoo, S., Ichoku, C., Kahn, R., and Eck, T. F.: Global evaluation of the Collection 5 MODIS dark-target aerosol products over land, Atmos. Chem. Phys., 10, 10399–10420, doi:10.5194/acp-10-10399-2010, 2010. 9126

Lipsky, E. M. and Robinson, A. L.: Effects of dilution on fine particle mass and partitioning of semivolatile organics in diesel exhaust and wood smoke, Environ. Sci. Technol., 40, 155–162, doi:10.1021/Es050319p, 2006. 9111

Madronich, S., McKenzie, R. E., Bjorn, L. O., and Caldwell, M. M.: Changes in biologically active ultraviolet radiation reaching the earth's surface, J. Photoch. Photobio. B, 46, 5–19, 1998. 9114

May, A. A., Levin, E. J. T., Hennigan, C. J., Riipinen, I., Lee, T., Collett Jr., J. L., Jimenez, J. L., Kreidenweis, S. M., and Robinson, A. L.: Gas-particle partitioning of primary organic aerosol emissions: 3. Biomass burning, J. Geophys. Res.-Atmos., 118, 11327–11338, doi:10.1002/jgrd.50828, 2013. 9111, 9122, 9129, 9159

Mei, L., Xue, Y., de Leeuw, G., Guang, J., Wang, Y., Li, Y., Xu, H., Yang, L., Hou, T., He, X., Wu, C., Dong, J., and Chen, Z.: Integration of remote sensing data and surface observations to estimate the impact of the Russian wildfires over Europe and Asia during August 2010, Biogeosciences, 8, 3771–3791, doi:10.5194/bg-8-3771-2011, 2011. 9113

Menut, L., Bessagnet, B., Khvorostyanov, D., Beekmann, M., Blond, N., Colette, A., Coll, I., Curci, G., Foret, G., Hodzic, A., Mailler, S., Meleux, F., Monge, J.-L., Pison, I., Siour, G., Turquety, S., Valari, M., Vautard, R., and Vivanco, M. G.: CHIMERE 2013: a model for regional

ACPD
15, 9107–9172, 2015

atmospheric composition modelling, Geosci. Model Dev., 6, 981–1028, doi:10.5194/gmd-6-981-2013, 2013. 9114, 9119, 9120

Mielonen, T., Portin, H. J., Komppula, M., Leskinen, A., Tamminen, J., Ialongo, I., Hakkarainen, J., Lehtinen, K. E. J., and Arola, A.: Biomass burning aerosols observed in Eastern Finland during the Russian wildfires in summer 2010 – Part 2: Remote sensing, Atmos. Environ., 45, 279–287, 2011. 9125

Murphy, B. N. and Pandis, S. N.: Simulating the formation of semivolatile primary and secondary organic aerosol in a regional chemical transport model, Environ. Sci. Technol., 43, 4722–4728, doi:10.1021/es803168a, 2009. 9112

Murphy, B. N., Donahue, N. M., Fountoukis, C., Dall'Osto, M., O'Dowd, C., Kiendler-Scharr, A., and Pandis, S. N.: Functionalization and fragmentation during ambient organic aerosol aging: application of the 2-D volatility basis set to field studies, Atmos. Chem. Phys., 12, 10797–10816, doi:10.5194/acp-12-10797-2012, 2012. 9142

Nenes, A., Pilinis, C., and Pandis, S.: ISORROPIA: a new thermodynamic model for inorganic multicomponent atmospheric aerosols, Aquat. Geochem., 4, 123–152, 1998. 9115

Ortega, A. M., Day, D. A., Cubison, M. J., Brune, W. H., Bon, D., de Gouw, J. A., and Jimenez, J. L.: Secondary organic aerosol formation and primary organic aerosol oxidation from biomass-burning smoke in a flow reactor during FLAME-3, Atmos. Chem. Phys., 13, 11551–11571, doi:10.5194/acp-13-11551-2013, 2013. 9111, 9124, 9129

Pankow, J.: An absorption model of the gas/aerosol partitioning involved in the formation of secondary organic aerosol, Atmos. Environ., 28, 189–193, 1994. 9121

Péré, J. C., Bessagnet, B., Mallet, M., Waquet, F., Chiapello, I., Minvielle, F., Pont, V., and Menut, L.: Direct radiative effect of the Russian wildfires and its impact on air temperature and atmospheric dynamics during August 2010, Atmos. Chem. Phys., 14, 1999–2013, doi:10.5194/acp-14-1999-2014, 2014. 9114

Petrenko, M., Kahn, R., Chin, M., Soja, A., Kucsera, T., and Harshvardhan: The use of satellite-measured aerosol optical depth to constrain biomass burning emissions source strength in the global model GOCART, J. Geophys. Res., 117, D18212, doi:10.1029/2012JD017870, 2012. 9111

Popovicheva, O. B., Kireeva, E. D., Persiantseva, N. M., Timofeev, M. A., Kistler, M., Kopeikin, V. M., and Kasper-Giebl, A.: Physicochemical characterization of smoke aerosol during large-scale wildfires: extreme event of August 2010 in Moscow, Atmos. Environ., 96, 405–414, doi:10.1016/j.atmosenv.2014.03.026, 2014. 9113, 9138

ACPD
15, 9107–9172, 2015

Portin, H. J., Mielonen, T., Leskinen, A., Arola, A., Pärjälä, E., Romakkaniemi, S., Laaksonen, A., Lehtinen, K. E. J., and Komppula, M.: Biomass burning aerosols observed in Eastern Finland during the Russian wildfires in summer 2010 – Part 1: In-situ aerosol characterization, Atmos. Environ., 47, 269–278, doi:10.1016/j.atmosenv.2011.10.067, 2012. 9125, 9130, 9138

Pöschl, U., Rose, D., and Andreae, M. O.: Climatologies of cloud-related aerosols – Part 2: Particle hygroscopicity and cloud condensation nuclei activity, in: Clouds in the Perturbed Climate System, edited by: Heintzenberg, J. and Charlson, R. J., MIT Press, Cambridge, ISBN 978-0-262-012874, 58–72, 2009. 9143

Pun, B. K., Seigneur, C., and Lohmann, K.: Modeling secondary organic aerosol formation via multiphase partitioning with molecular data, Environ. Sci. Technol., 40, 4722–4731, 2006. 9120

Reid, J. S., Eck, T. F., Christopher, S. A., Koppmann, R., Dubovik, O., Eleuterio, D. P., Holben, B. N., Reid, E. A., and Zhang, J.: A review of biomass burning emissions part III: intensive optical properties of biomass burning particles, Atmos. Chem. Phys., 5, 827–849, doi:10.5194/acp-5-827-2005, 2005. 9115

Remer, L. A., Kaufman, Y. J., Tanre, D., Mattoo, S., Chu, D. A., Martins, J. V., Li, R.-R., Ichoku, C., Levy, R. C., Kleidman, R. G., Eck, T. F., Vermote, E., and Holben, B. N.: The MODIS aerosol algorithm, products, and validation, J. Atmos. Sci., 62, 947–973, 2005. 9126

Robinson, A. L., Donahue, N. M., Shrivastava, M. K., Weitkamp, E. A., Sage, A. M., Grieshop, A. P., Lane, T. E., Pierce, J. R., and Pandis, S. N.: Rethinking organic aerosols: semivolatile emissions and photochemical aging, Science, 315, 1259–1262, doi:10.1126/science.1133061, 2007. 9111, 9119, 9140

Saleh, R., Hennigan, C. J., McMeeking, G. R., Chuang, W. K., Robinson, E. S., Coe, H., Donahue, N. M., and Robinson, A. L.: Absorptivity of brown carbon in fresh and photo-chemically aged biomass-burning emissions, Atmos. Chem. Phys., 13, 7683–7693, doi:10.5194/acp-13-7683-2013, 2013. 9143

Saleh, R., Robinson, E. S., Tkacik, D. S., Ahern, A. T., Liu, S., Aiken, A. C., Sullivan, R. C., Presto, A. A., Dubey, M. K., Yokelson, R. J., Donahue, N. M., and Robinson, A. L.: Brownness of organics in aerosols from biomass burning linked to their black carbon content, Nat. Geosci., 7, 647–650, doi:10.1038/ngeo2220, 2014. 9110

Seinfeld, J. H., and Pandis, S. N.: Atmospheric Chemistry and Physics: from Air Pollution to Climate Change, 2nd edn., Wiley-Interscience, J. Wiley & Sons, Inc., New York, 2006. 9122

ACPD
15, 9107–9172, 2015

Shrivastava, M. K., Lipsky, E. M., Stanier, C. O., and Robinson, A. L.: Modeling semivolatile organic aerosol mass emissions from combustion systems, Environ. Sci. Technol., 40, 2671–2677, doi:10.1021/es0522231, 2006. 9111, 9121

Shrivastava, M., Fast, J., Easter, R., Gustafson Jr., W. I., Zaveri, R. A., Jimenez, J. L., Saide, P., and Hodzic, A.: Modeling organic aerosols in a megacity: comparison of simple and complex representations of the volatility basis set approach, Atmos. Chem. Phys., 11, 6639–6662, doi:10.5194/acp-11-6639-2011, 2011. 9112

Sinha, P., Hobbs, P. V., Yokelson, R. J., Blake, D. R., Gao, S., and Kirchstetter, T. W.: Distribution of trace gases and aerosols during the dry biomass burning season in southern Afirca, J. Geophys. Res., 108, D17, doi:10.1029/2003JD003691, 2003. 9110

Skamarock, W. C., Klemp, J. B., Dudhia, J., Gill, D. O., Barker, D. M., Wang, W., and Powers, J. G.: A description of the Advanced Research WRF Version 2, NCAR Tech Notes-468+STR, Boulder, Colorado, USA, 2005. 9116

Sofiev, M., Vankevich, R., Lotjonen, M., Prank, M., Petukhov, V., Ermakova, T., Koskinen, J., and Kukkonen, J.: An operational system for the assimilation of the satellite information on wild-land fires for the needs of air quality modelling and forecasting, Atmos. Chem. Phys., 9, 6833–6847, doi:10.5194/acp-9-6833-2009, 2009. 9117

Sofiev, M., Ermakova, T., and Vankevich, R.: Evaluation of the smoke-injection height from wild-land fires using remote-sensing data, Atmos. Chem. Phys., 12, 1995–2006, doi:10.5194/acp-12-1995-2012, 2012. 9119

Strand, T. M., Larkin, N., Craig, K. J., Raffuse, S., Sullivan, D., Solomon, R., Rorig, M., Wheeler, N., and Pryden, D.: Analyses of BlueSky Gateway $PM_{2.5}$ predictions during the 2007 southern and 2008 northern California fires, J. Geophys. Res., 117, D17301, doi:10.1029/2012JD017627, 2012. 9110

Stevanovic, S., Miljevic, B., Surawski, N. C., Fairfull-Smith, K. E., Bottle, S. E., Brown, R., and Ristovski, Z. D.: Influence of Oxygenated Organic Aerosols (OOAs) on the oxidative potential of diesel and biodiesel particulate matter, Environ. Sci. Technol., 47, 7655–7662, doi:10.1021/es4007433, 2013. 9143

Stohl, A., Williams, E., Wotawa, G., and Kromp-Kolb, H.: A European inventory of soil nitric oxide emissions and the effect of these emissions on the photochemical formation of ozone, Atmos. Environ., 30, 3741–3755, doi:10.1016/1352-2310(96)00104-5, 1996. 9115

Tsimpidi, A. P., Karydis, V. A., Zavala, M., Lei, W., Molina, L., Ulbrich, I. M., Jimenez, J. L., and Pandis, S. N.: Evaluation of the volatility basis-set approach for the simulation of organic

ACPD
15, 9107–9172, 2015

aerosol formation in the Mexico City metropolitan area, Atmos. Chem. Phys., 10, 525–546, doi:10.5194/acp-10-525-2010, 2010. 9112
Vakkari, V., Kerminen, V.-M., Beukes, J. P., Tiitta, P., van Zyl, P. G., Josipovic, M., Venter, A. D., Jaars, K., Worsnop, D. R., Kulmala, M., and Laakso, L.: Rapid changes in biomass burning aerosols by atmospheric oxidation, Geophys. Res. Lett., 41, 2644–2651, doi:10.1002/2014GL059396, 2014. 9112, 9133, 9142
van der Werf, G. R., Randerson, J. T., Giglio, L., Collatz, G. J., Mu, M., Kasibhatla, P. S., Morton, D. C., DeFries, R. S., Jin, Y., and van Leeuwen, T. T.: Global fire emissions and the contribution of deforestation, savanna, forest, agricultural, and peat fires (1997–2009), Atmos. Chem. Phys., 10, 11707–11735, doi:10.5194/acp-10-11707-2010, 2010. 9119, 9121
van Donkelaar, A., Martin, R. V., Levy, R. C., da Silva, A. M., Krzyzanowski, M., Chubarova, N. E., Semutnikova, E., and Cohen, A. J.: Satellite-based estimates of ground-level fine particulate matter during extreme events: a case study of the Moscow fires in 2010, Atmos. Environ., 45, 6225–6232, 2011. 9136, 9137
Vautard, R., Bessagnet, B., Chin, M., and Menut, L.: On the contribution of natural aeolian sources to particulate matter concentrations in Europe: testing hypotheses with a modelling approach, Atmos. Environ., 39, 3291–3303, 2005. 9115
Vicente, A., Alves, C., Calvo, A. I., Fernandes, A. P., Nunes, T., Monteiro, C., Almeida, S. M., and Pio, C.: Emission factors and detailed chemical composition of smoke particles from the 2010 wildfire season, Atmos. Environ., 71, 295–303, doi:10.1016/j.atmosenv.2013.01.062, 2013. 9122
Wang, J., Christopher, S. A., Nair, U. S., Reid, J. S., Prins, E. M., Szykman, J., and Hand, J. L.: Mesoscale modeling of Central American smoke transport to the United States: 1. "Top-down" assessment of emission strength and diurnal variation impacts, J. Geophys. Res., 111, D05S17, doi:10.1029/2005JD006416, 2006. 9110
Wiedinmyer, C., Quayle, B., Geron, C., Belote, A., McKenzie, D., Zhang, X. Y., O'Neill, S., and Wynne, K. K.: Estimating emissions from fires in North America for air quality modeling, Atmos. Environ., 40, 3419–3432, 2006.
Witte, J. C., Douglass, A. R., da Silva, A., Torres, O., Levy, R., and Duncan, B. N.: NASA A-Train and Terra observations of the 2010 Russian wildfires, Atmos. Chem. Phys., 11, 9287–9301, doi:10.5194/acp-11-9287-2011, 2011. 9113, 9128
Wooster, M. J., Roberts, G., Perry, G. L. W., and Kaufman, Y. J.: Retrieval of biomass combustion rates and totals from fire radiative power observations: FRP derivation and calibration

ACPD
15, 9107–9172, 2015

relationships between biomass consumption and fire radiative energy release, J. Geophys. Res., 110, D24311, doi:10.1029/2005JD006318, 2005. 9117

Xu, X., Wang, J., Henze, D. K., Qu, W., and Kopacz, M.: Constraints on aerosol sources using GEOS-Chem adjoint and MODIS radiances, and evaluation with multisensor (OMI, MISR) data, J. Geophys. Res.-Atmos., 118, 6396–6413, doi:10.1002/jgrd.50515, 2013. 9138

Yokelson, R. J., Crounse, J. D., DeCarlo, P. F., Karl, T., Urbanski, S., Atlas, E., Campos, T., Shinozuka, Y., Kapustin, V., Clarke, A. D., Weinheimer, A., Knapp, D. J., Montzka, D. D., Holloway, J., Weibring, P., Flocke, F., Zheng, W., Toohey, D., Wennberg, P. O., Wiedinmyer, C., Mauldin, L., Fried, A., Richter, D., Walega, J., Jimenez, J. L., Adachi, K., Buseck, P. R., Hall, S. R., and Shetter, R.: Emissions from biomass burning in the Yucatan, Atmos. Chem. Phys., 9, 5785–5812, doi:10.5194/acp-9-5785-2009, 2009. 9112

Zhang, Q. J., Beekmann, M., Drewnick, F., Freutel, F., Schneider, J., Crippa, M., Prevot, A. S. H., Baltensperger, U., Poulain, L., Wiedensohler, A., Sciare, J., Gros, V., Borbon, A., Colomb, A., Michoud, V., Doussin, J.-F., Denier van der Gon, H. A. C., Haeffelin, M., Dupont, J.-C., Siour, G., Petetin, H., Bessagnet, B., Pandis, S. N., Hodzic, A., Sanchez, O., Honoré, C., and Perrussel, O.: Formation of organic aerosol in the Paris region during the MEGAPOLI summer campaign: evaluation of the volatility-basis-set approach within the CHIMERE model, Atmos. Chem. Phys., 13, 5767–5790, doi:10.5194/acp-13-5767-2013, 2013. 9112, 9119, 9124

Zhang, S., Penner, J. E., and Torres, O.: Inverse modeling of biomass burning emissions using Total Ozone Mapping Spectrometer aerosol index for 1997, J. Geophys. Res., 110, D21306, doi:10.1029/2004JD005738, 2005. 9138

Zhang, Y., Huang, J.-P., Henze, D. K., and Seinfeld, J. H.: Role of isoprene in secondary organic aerosol formation on a regional scale, J. Geophys. Res.-Atmos., 112, D20207, doi:10.1029/2007JD008675, 2007. 9120

ACPD
15, 9107–9172, 2015

Table 1. Biomass burning emission factors (β, $g\,kg^{-1}$) specified in the emission model (see Eq. 1) for different types of vegetative land cover. The data are based on Andreae and Merlet (2001) and subsequent updates.

	agricultural burning	grassland	forest
OC	4.2	3.1	7.7
BC	0.42	0.55	0.58
CO	95	65	115
NMHC	9.9	5.5	8.7
NO_x	2.44	2.49	3.10

ACPD
15, 9107–9172, 2015

Table 2. Simulation settings for the different modelling scenarios with emissions from fires. The POA oxidation schemes I and II are based on the parameterizations described in Grieshop et al. (2009a) and Jathar et al. (2014), respectively (see Sect. 2.4.2). The corresponding volatility distributions are specified in Table 3. Note that along with the simulations based on the "fire" scenarios listed in the table, an additional model run ("BGR") was made to simulate "background" conditions in the absence of fires (see Sect. 2.7).

Modeling scenario	k_{OH}, $cm^3\,s^{-1}$	POA oxidation scheme	Volatility distribution type
STN	N/A	N/A	N/A
VBS-1	2×10^{-11}	I	A
VBS-2	2×10^{-11}	I	B
VBS-3	2×10^{-11}	II	A
VBS-4	4×10^{-11}	I	A
VBS-5	N/A	N/A	A

ACPD
15, 9107–9172, 2015

Table 3. Volatility distributions (f_i) used in the different simulation scenarios (see Table 1). The distributions are based on the data by May et al. (2013) and were used together with the recommended values of the accommodation coefficient and the enthalpies (γ = 1.0, H_{vap} = $85 - 4 \log C_i^*$).

	Volatility distribution type	
C_i^*	A	B
10^{-2}	0.2	0.1
10^{-1}	0.0	0.0
1	0.1	0.05
10	0.1	0.05
10^2	0.2	0.2
10^3	0.1	0.15
10^4	0.3	0.45

ACPD
15, 9107–9172, 2015

Table 4. Characteristics of the simulation data (after bias correction) compared to air pollution measurements at monitoring stations in the Moscow region. F_α are the optimal estimates for the fire emission correction factor (see Eq. 1) derived from PM_{10} data; the geometric SD characterizing uncertainties in F_α are given in parentheses. $\overline{PM_{10}}$ is the mean PM_{10} concentration over the study period. $[\Delta PM_{10}/\Delta CO]_{fit}$ is the normalized excess mixing ratio evaluated as the slope of a linear fit to the relationship between perturbations of CO and PM_{10} concentrations on days affected by fire emissions (see also Fig. 7).

Characteristic	Observations	Simulation scenario					
		STN	VBS-1	VBS-2	VBS-3	VBS-4	VBS-5
F_α	N/A	1.03(1.09)	1.03(1.06)	1.05(1.09)	1.12(1.13)	0.95(1.08)	1.54(1.11)
$\overline{PM_{10}}$ [$\mu g\,m^{-3}$]	1.23×10^2	1.02×10^2	1.04×10^2	1.06×10^2	1.00×10^2	1.05×10^2	1.00×10^2
RMSE [$\mu g\,m^{-3}$]	N/A	8.15×10^1	8.01×10^1	7.89×10^1	8.33×10^1	7.87×10^1	8.40×10^1
r	N/A	0.86	0.86	0.86	0.85	0.86	0.85
$[\Delta PM_{10}/\Delta CO]_{fit}$, [$g\,g^{-1}$]	6.94×10^{-2}	6.68×10^{-2}	6.71×10^{-2}	6.67×10^{-2}	6.78×10^{-2}	6.71×10^{-2}	6.73×10^{-2}

ACPD
15, 9107–9172, 2015

Table 5. Characteristics of simulation data (after bias correction) compared to air pollution measurements at the Maaherrankatu site in Kuopio.

Characteristic	Observations	Simulation scenario					
		STN	VBS-1	VBS-2	VBS-3	VBS-4	VBS-5
$\overline{PM_{10}}$ [$\mu g\,m^{-3}$]	1.75×10^{1}	1.58×10^{1}	1.74×10^{1}	1.81×10^{1}	1.59×10^{1}	1.74×10^{1}	1.55×10^{1}
RMSE [$\mu g\,m^{-3}$]	N/A	7.25	6.26	6.74	7.44	6.35	7.65
r	N/A	0.91	0.89	0.88	0.88	0.89	0.91
$[\Delta PM_{10}/\Delta CO]_{fit}$, [$g\,g^{-1}$]	1.30×10^{-1}	7.32×10^{-2}	1.13×10^{-1}	1.34×10^{-1}	8.43×10^{-1}	1.16×10^{-1}	6.64×10^{-2}

ACPD
15, 9107–9172, 2015

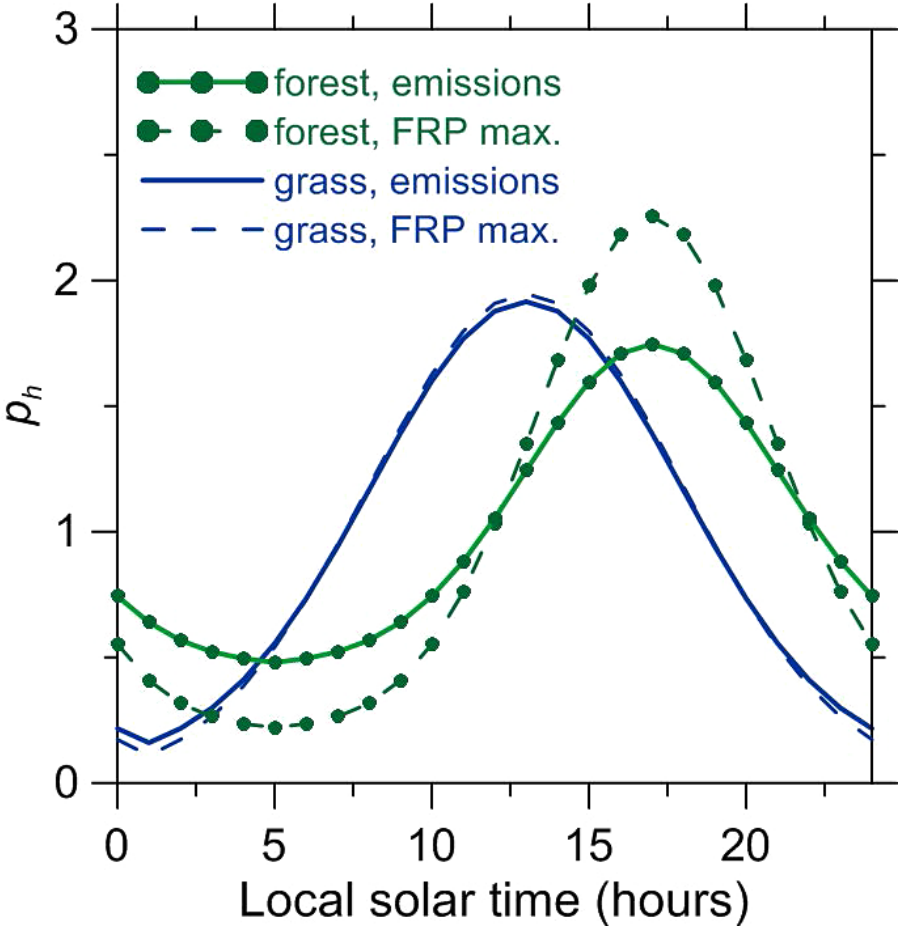

Figure 1. Diurnal profiles of fire emissions ($h_e(t)$) and daily FRP maximums ($h_m(t)$) used in the emission model (see Eqs. 1 and 2).

ACPD
15, 9107–9172, 2015

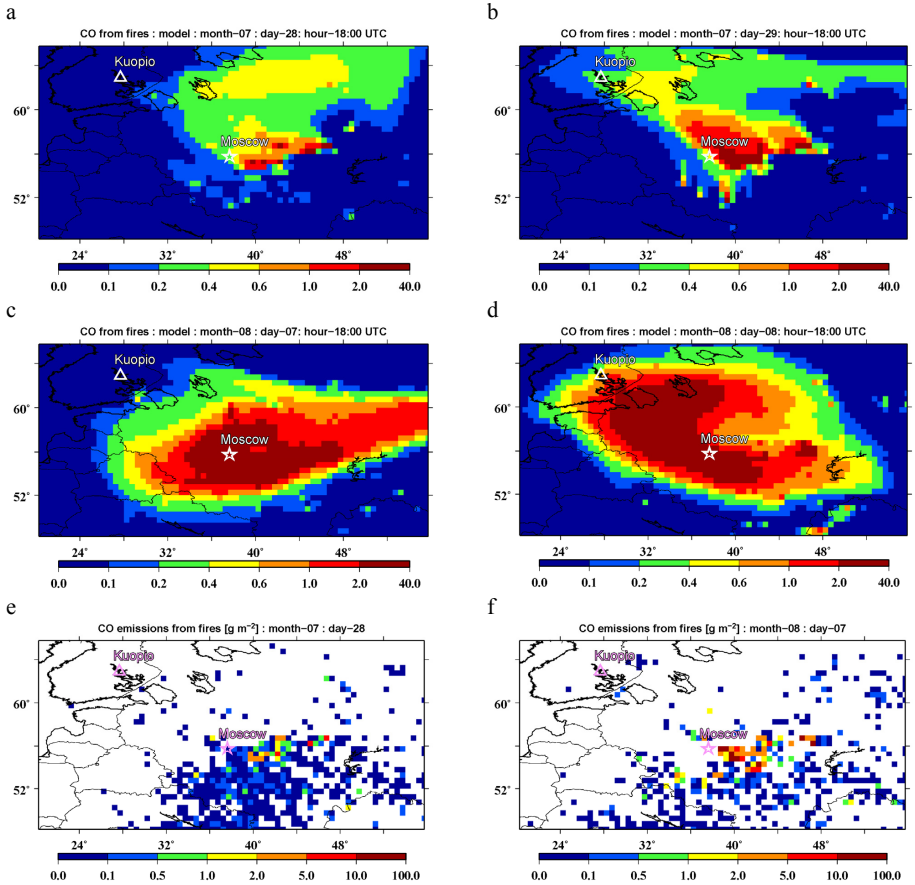

Figure 2. Simulated near-surface concentration ($mg\,m^{-3}$) of fire-emitted CO at 18:00 UTC on **(a, b)** 28 and 29 July and on **(c, d)** 7 and 8 August 2010, respectively, along with spatial distributions of CO amounts ($g\,m^{-2}$) emitted from fires on **(e)** 28 July and **(f)** 7 August 2010.

ACPD
15, 9107–9172, 2015

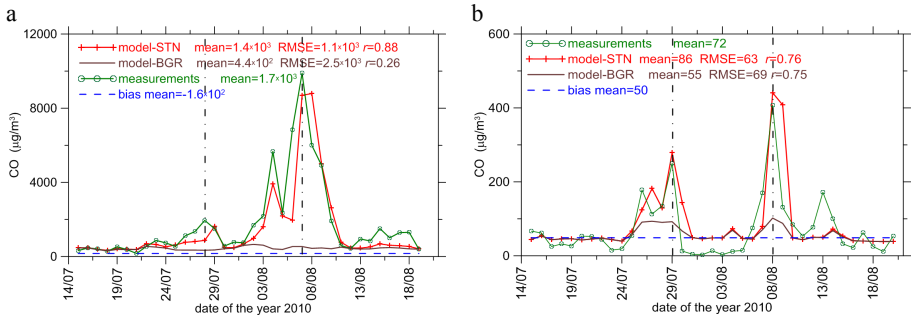

Figure 3. Time series of daily CO concentrations in Moscow **(a)** and in Kuopio **(b)**. The CO concentration for the simulation scenario "STN" (see the red lines with crosses) are obtained by taking into account both anthropogenic and fire emissions (as explained in Sect. 2.7), while that for the "BGR" run (see the solid brown lines) reflects only anthropogenic CO emissions (along with other sources contributing to the boundary conditions for CO). The dashed blue lines depict the model bias (representing the systematic difference between the simulations and measurements on days not affected by fires); note that a negative bias (specifically, in the plot "a") is shown with the opposite sign. The measurement data (from Mosecomonitoring stations and the Maaherrankatu site in Kuopio) are shown by green lines. The vertical dashed lines indicate the CO concentrations observed **(a)** in Kuopio on 29 July and 8 August and **(b)** in Moscow on 28 July and 7 August.

ACPD
15, 9107–9172, 2015

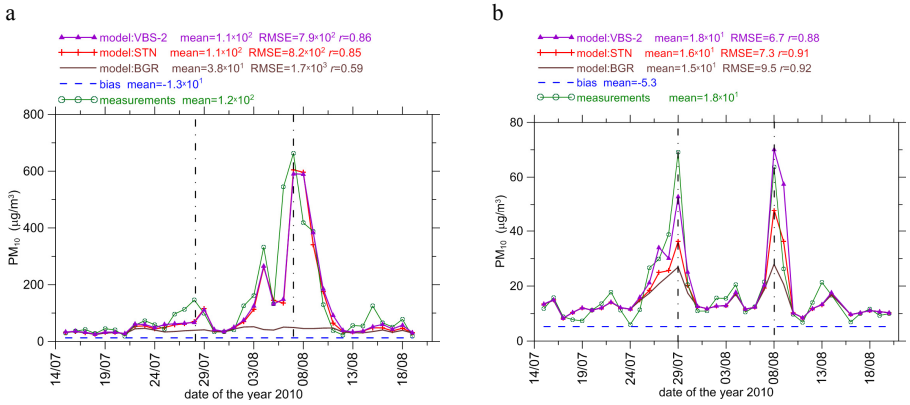

Figure 4. The same as in Fig. 3 but for PM_{10} concentrations, except that in addition to results for the STN and BGR runs, this figure shows (by a purple line) results for the VBS-2 run.

ACPD
15, 9107–9172, 2015

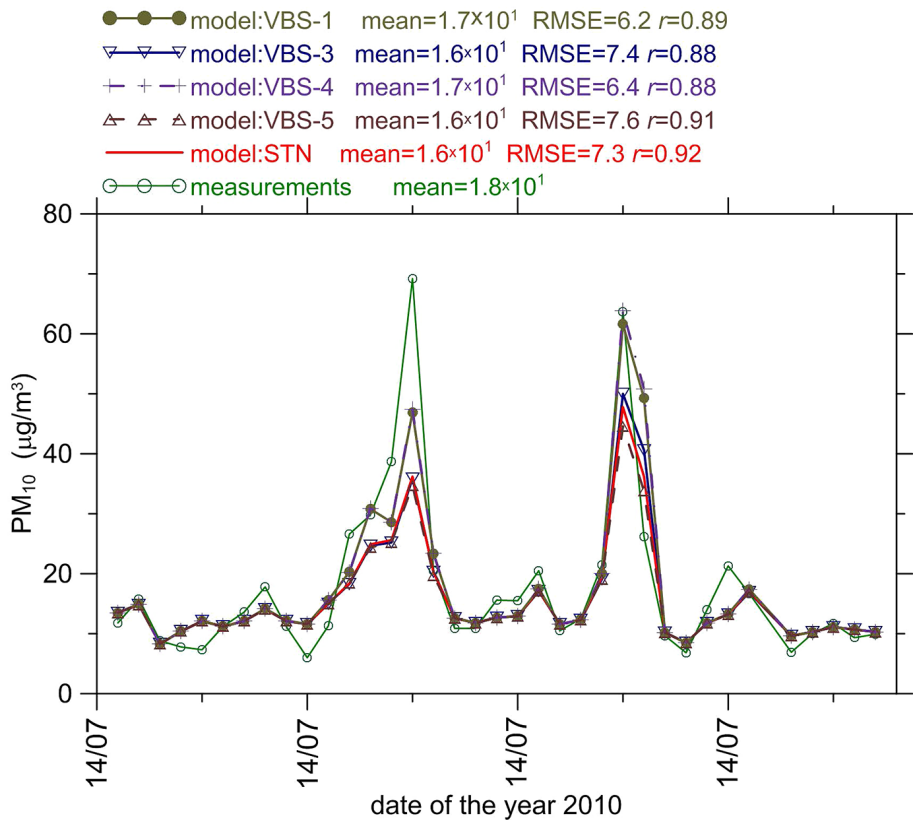

Figure 5. Time series of daily PM_{10} concentrations according to different simulation scenarios in comparison with measurements in Kuopio. Note that the time series for the VBS-2 scenario, which is shown in Fig. 4b, is omitted in this figure.

ACPD
15, 9107–9172, 2015

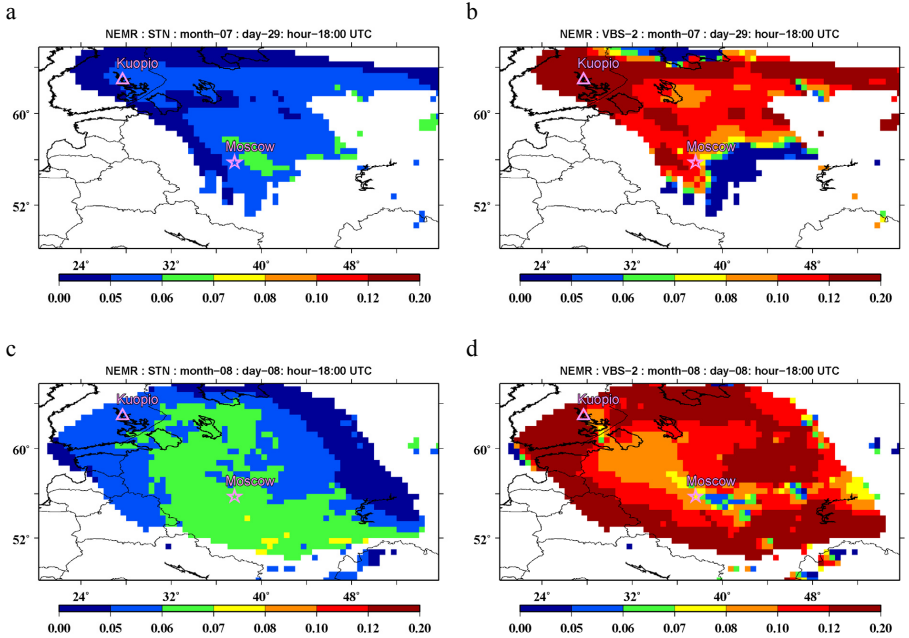

Figure 6. Normalized excess mixing ratio (NEMR) calculated as the ratio of near-surface mass concentrations of PM_{10} and CO ($g\,g^{-1}$) originating from the fires. The NEMR values are shown only in the grid cells with CO concentration exceeding 100 $\mu g\,m^{-3}$ for 29 July **(a, b)** and 8 August **(c, d)** 2010 according to the STN **(a, c)** and VBS-2 **(b, d)** scenarios.

ACPD
15, 9107–9172, 2015

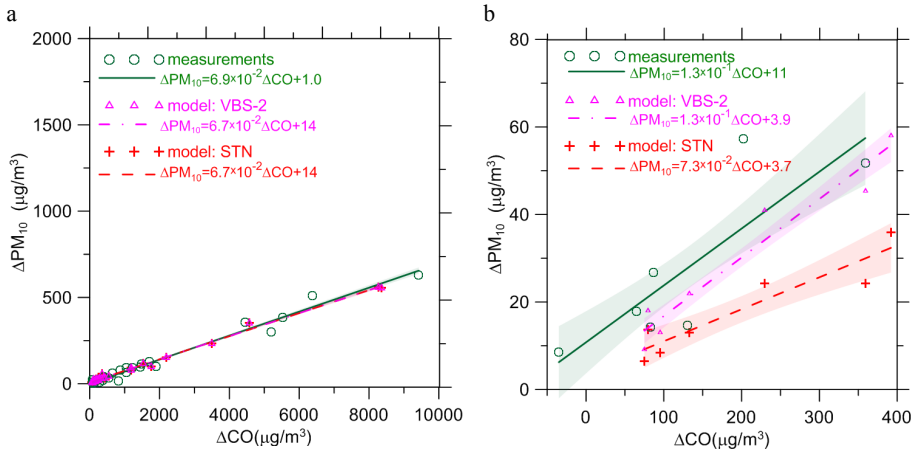

Figure 7. Scatter plots of the enhancements of PM_{10} and CO concentrations (ΔPM_{10} and ΔCO) in **(a)** Moscow and **(b)** Kuopio on days affected by smoke from fires. Note that the relative scales of the ΔPM_{10} and ΔCO values are the same on both plots. The slope of a linear fit to the data provides an estimate of NEMR (see Sect. 3.1). The shaded areas depict uncertainties of the fits at the 68 % confidence level.

ACPD
15, 9107–9172, 2015

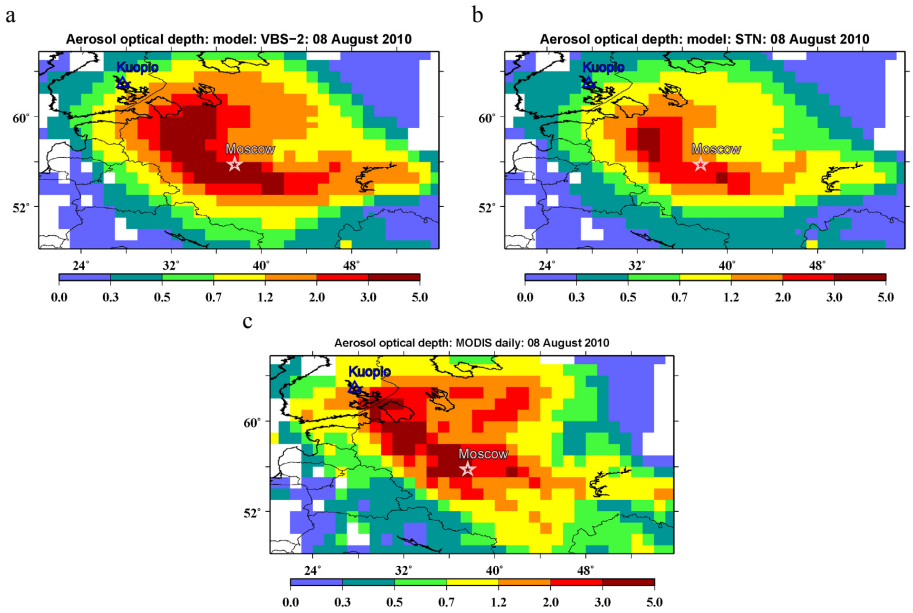

Figure 8. Spatial distributions of AOD at 550 nm on 8 August 2010 according to simulations for the scenarios "VBS-2" **(a)** and "STN" **(b)** in comparison with the MODIS measurement data **(c)**.

ACPD
15, 9107–9172, 2015

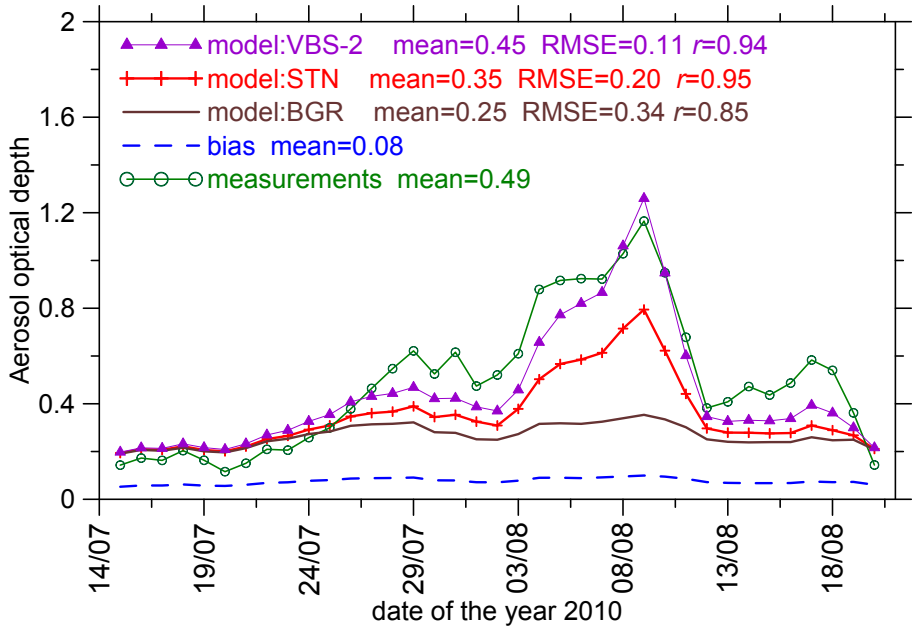

Figure 9. Time series of AOD at 550 nm obtained from simulations made with different scenarios and derived from the MODIS measurements. The daily data are averaged over the whole study region (see Fig. 8).

ACPD
15, 9107–9172, 2015

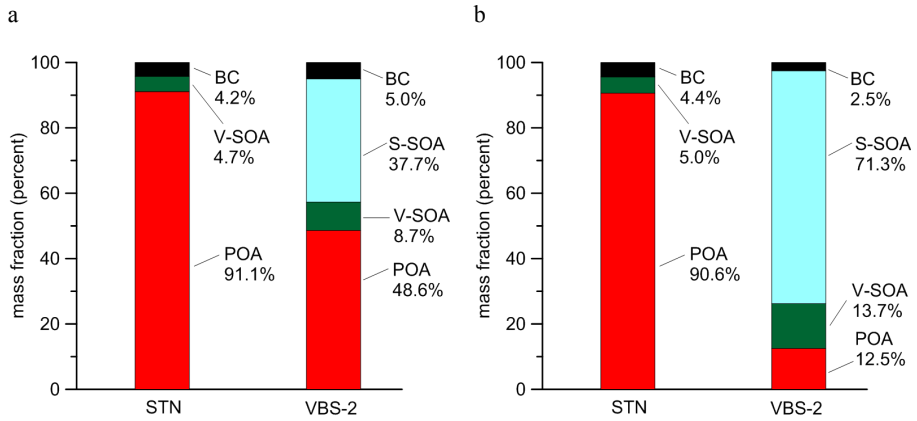

Figure 10. Composition of BB aerosol according to the simulations scenarios "STN" and "VBS-2" **(a)** in Moscow (at 18:00 UTC on 7 August 2010) and **(b)** in Kuopio (at 18:00 UTC on 8 August 2010).

ACPD
15, 9107–9172, 2015

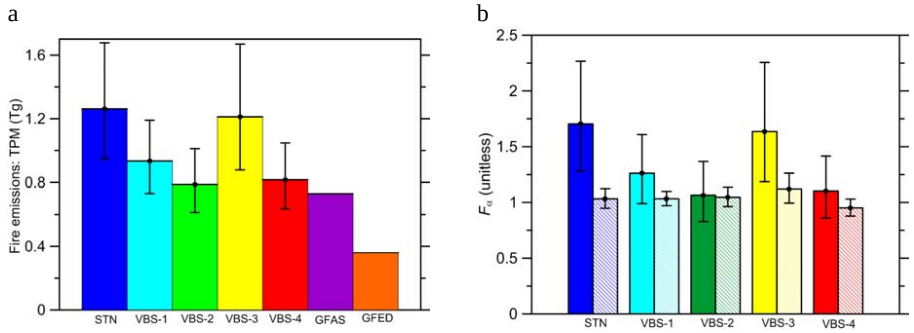

Figure 11. (a) Top-down estimates (in Tg) of total BB aerosol emissions from the study region in the period from 1 July to 31 August 2010 according to different simulation scenarios and in comparison with total particulate matter (TPM) emission data from the GFASv1.0 and GFED3.1 inventories. The estimates are derived from the MODIS AOD measurements. **(b)** The corresponding optimal estimates of F_α derived from MODIS (boxes with solid filling) measurements in comparison with corresponding estimates (boxes with dashed filling) obtained from ground-based measurements in the Moscow region. Note that the estimates for the "unrealistic" scenario "VBS-5", which would exceed the axis limits (see Sect. 3.4), are not shown.

ACPD
15, 9107–9172, 2015